

## Chemical weathering of the Panola Granite: Solute and regolith elemental fluxes and the weathering rate of biotite

ART F. WHITE<sup>1\*</sup>, ALEX E. BLUM<sup>2</sup>, MARJORIE S. SCHULZ<sup>1</sup>, THOMAS G. HUNTINGTON<sup>3</sup>, NORMAN E. PETERS<sup>3</sup>  
AND DAVID A. STONESTROM<sup>1</sup>

<sup>1</sup> U. S. Geological Survey, Menlo Park, CA 94025 USA

<sup>2</sup> U. S. Geological Survey, Boulder, CO 80303 USA

<sup>3</sup> U. S. Geological Survey, Atlanta, GA 30360 USA

\* corresponding author: afwhite@usgs.gov

**Abstract**—Present-day elemental and mineral weathering rates based on solute fluxes are compared quantitatively to past long-term rates determined from solid-state elemental fractionation in a saprolitic granite regolith at Panola, Georgia, USA. Saturated fluid flow across a low-permeability kaolin duripan controls the rate of steady-state unsaturated flow in the underlying saprolite. Water and Cl mass balances and experimental conductivities produce a minimum fluid flux density of  $8 \times 10^{-2}$  m yr<sup>-1</sup> and a fluid residence time of 12 years. Solute Si flux, based on pore water concentrations and infiltration rates, is 27 mmol yr<sup>-1</sup>, compared to a long-term flux rate of 17 mmol yr<sup>-1</sup>, based on regolith Si loss and reported <sup>36</sup>Cl dating of the regolith surface. Similarities in short- and long-term fluxes imply that parameters influencing silicate weathering, including precipitation, temperature, and vegetative cover, while not necessarily constant, have not significantly impacted Si leaching rates during the last several hundred thousand years.

Linear decreases in solid-state Mg with decreasing regolith depth permit the calculation of the long-term biotite weathering rate under isovolumetric steady-state weathering conditions. A rate constant of  $3 \times 10^{-17}$  moles m<sup>-2</sup> s<sup>-1</sup> is up to 5 orders of magnitude slower than that reported for experimental dissolution of biotite, implying very different reaction kinetics during natural weathering. Short-term biotite weathering fails to produce expected increases in solute Mg and K concentrations with increasing depth and fluid residence times in the regolith. This discrepancy indicates that ion exchange disequilibrium and open-system biologic uptake in an aggrading forest ecosystem are of sufficient magnitudes to overwhelm solute fluxes resulting from biotite weathering.

### 1. INTRODUCTION

The quantification of natural silicate weathering rates has important implications in a diverse range of geochemical issues, including the neutralization of acid precipitation, the release rates of macronutrients such as K and Ca in forested catchments, and the linkage between weathering rates, CO<sub>2</sub> draw-down, and long-term climate change. In addressing these issues, extensive efforts have been directed at determining silicate weathering mechanisms and rates based on detailed experiments that involve generally well-characterized silicate minerals. In many cases, the success of these efforts has surpassed our present ability to verify their applicability to natural weathering processes.

Most quantitative estimates of natural silicate weathering rates are derived by simple input-output models, which fall conceptually into two categories (White, 1995). Short-term reaction rates are calculated from solute fluxes derived most commonly from rates of regolith infiltration (Swodoba-Colberg and Drever, 1993; Murphy et al., 1998), watershed solute balances (Velbel, 1985; Pačes, 1986), and from solute increases observed along ground water flow paths

(White and Claassen, 1978; Kenoyer and Bowser, 1992). The determination of such rates commonly requires an extensive monitoring network characterizing fluid flow and solute compositions. In such studies, it is commonly difficult to document the *in situ* parameters that control silicate reaction rates, including reactive mineral surface areas and hydrologic flow paths and heterogeneities. Such monitoring efforts are commonly short-term, one to several years, which may or may not approach the actual fluid residence times in these systems. Extrapolation of such short-term rates to longer times, therefore, is susceptible to effects of changing climate, vegetation, and anthropogenic influences.

Long-term reaction rates are calculated from differences between elemental or mineral compositions in the initial protolith and the weathered regolith. While extensive data in the soil literature document such compositional differences, relatively few studies have tied these changes to quantitative mineral weathering rates (Sverdrup and Warfvinge, 1995; White et al., 1996; White et al., 2001). These rates are averages for the duration of protolith weathering, commonly tens of thousands to millions of years. Studies confined solely to the solid-state provide minimal infor-

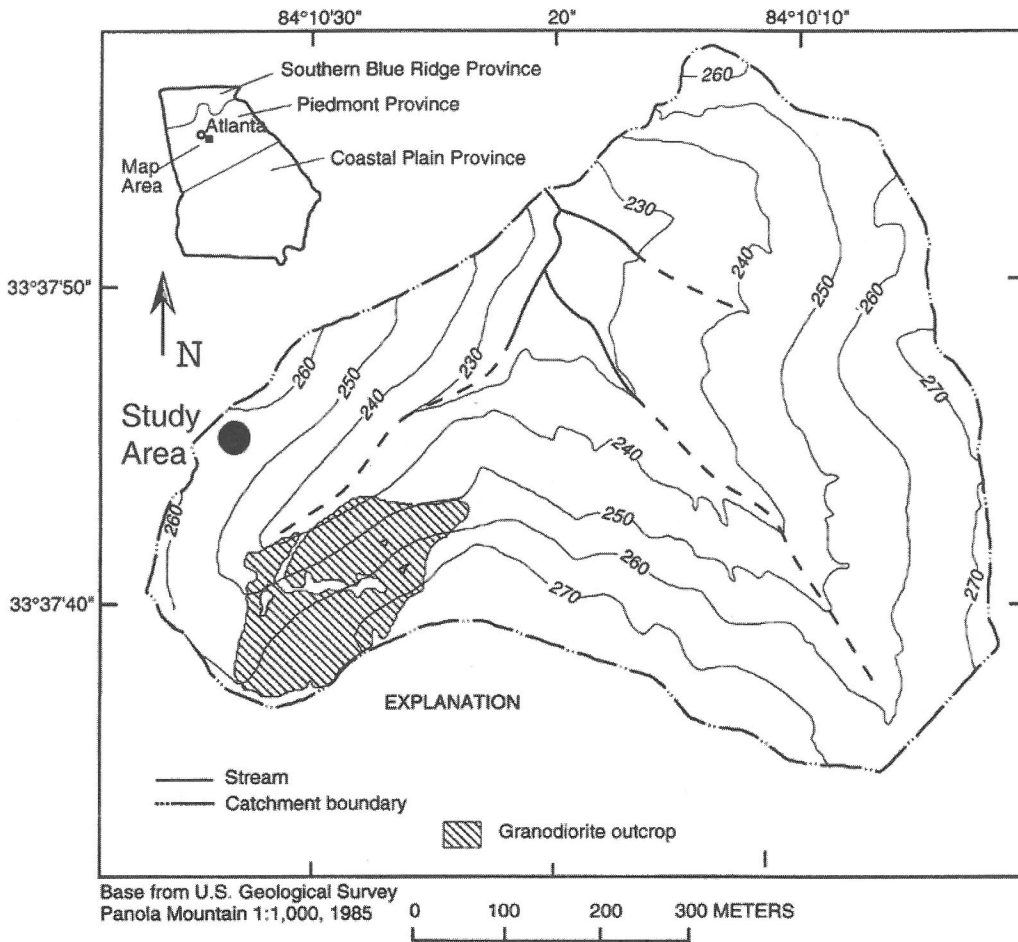


Fig. 1. Location map showing the ridge top sampling site in the Panola watershed. Dashed area represents outcrop areas of the Panola Granodiorite.

mation of long-term hydrochemical processes that have led to observed weathering rates. Weathering rates can change over long times due to the decreasing availability of reactive surfaces and increasing secondary clay and oxide phases which alter permeability, wetted mineral surface areas, and mineral reaction affinities.

Additional insights into natural weathering are derived from direct comparisons of present short-term and past long-term rates for the same regolith. Significant differences imply errors in the assumptions used in calculating weathering rates and/or fundamental changes in the actual rates over time (White, 1995). Current silicate weathering rates, based on watershed solute fluxes in post-glacial watersheds ( $< 1 \times 10^4$  yrs) in North America and northern Europe, are estimated to be up to a factor of 3 times faster than long-term past

weathering rates based on cation and mineral depletions in watershed soils (April et al., 1986; Kirkwood and Nesbitt, 1991; Land et al., 1999). These differences are attributed to the impacts of acidic precipitation on contemporary weathering rates.

In comparing long-term weathering rates for much older saprolites ( $> 10^5$  years) with watershed solute discharge in the Piedmont of the eastern USA, Cleaves (1993) concluded that present interglacial weathering rates are 2-5 times faster than for past periglacial periods. This difference is attributed to past periods of lower precipitation, colder temperatures, and lower soil gas  $\text{CO}_2$ . In contrast, Pavich et al. (1995) concluded that long-term rates of saprolite formation in the Virginia Piedmont are comparable with current-weathering rates based on stream solute fluxes. Rates of saprolite formation are also found

similar to current weathering rates based on watershed discharge in the Luquillo Mountains of Puerto Rico, an area which has been subject to only minor long-term climate fluctuations (White et al., 1998).

The present study details methods for deriving both short-term weathering rates based on present-day soil water fluxes and past long-term weathering rates calculated from changes in regolith composition. These approaches are applied to a saprolitic weathering environment in the Georgia Piedmont of the eastern USA. The importance of heterogeneous permeabilities in estimating solute fluxes is investigated. Dissolution rates of biotite, derived from solid-state elemental distributions with depth in the regolith, are compared to experimental rates and rates determined for other natural systems. Finally, the impacts of biologic fluxes and cation exchange reactions on pore water chemistry, used to calculate contemporary weathering rates, are assessed.

## 2. FIELD SETTING AND METHODOLOGY

Panola Mountain Research Watershed is a 41-hectare watershed within the Panola Mountain State Conservation Park located in the Piedmont province of Georgia, USA (Fig. 1). Chemical weathering in the Panola watershed has been addressed in a number of studies (Grant, 1975; Nixon, 1981; Burns, 1998; Stonestrom et al., 1998; Schroeder and Mearl, 1999; White et al., 1999a,b; White et al. 2001). The average annual precipitation is 1.24 m and the mean annual air temperature is 18 °C. Land use records indicate the original forest was cut in the early 1800's and was farmed until the early 1900's (Huntington, 1995). The watershed is currently covered with a mixed deciduous/coniferous forest. Tree root densities are greatest within the upper meter of regolith, with a sparser distribution of roots penetrating to the bedrock surface.

The focus of the present study is a ridge top in the western quadrant of the watershed (Fig. 1), which is underlain by the 320 M yr old Panola Granite, described as a biotite-muscovite oligoclase-quartz-microcline granodiorite (Higgins et al., 1988). The ridge-top is an old erosion surface comparable in age to granodiorite surface exposures in the watershed dated at between 200-500 kyrs by  $^{36}\text{Cl}$  (Bierman et al., 1995). The ridge-top soils are highly weathered ultisols developed *in situ* from bedrock residuum and consist of a dense, dark red, unstructured clay-rich A horizon (~0.5 m thick), underlain by a less dense orange-brown B-horizon (~1 m thick). The underlying porous saprolite (~2-3 m thick) retains the original granodiorite texture and grades from friable saprock to competent bedrock

over an interval of several cm at a depth of 4.7 m.

Nested porous cup suction water samplers were installed at the bottom of holes augered to depths of 0.1 to 4.6 m in the ridge-top regolith and sampled bi-weekly to monthly from December 1991 to April of 1993. The site was also sampled during a LiBr tracer test in 1995 (Huntington et al., 1994). Water samples from the suction samplers were filtered in the laboratory, pH and alkalinity determined, and chemistry analyzed using ion chromatography and direct current plasma spectroscopy. Porous tip tensiometers with analogue gauges were installed at selected depth intervals at the site. Moisture samples were taken using a soil corer and measured for gravimetric water content. Soil and saprolite cores, taken at depths ranging from 0.78 to 2.35 m, were measured in the laboratory for saturated hydraulic conductivities using a falling head permeameter (Klute and Dirksen, 1986; Stonestrom et al., 1998).

Surface areas of bulk soil and saprolite, in addition to individual mineral separates, were determined by single point BET measurements using  $\text{N}_2$ . Mineral separates were split and sieved to retain the <2 mm fraction. Clay-size particles (<4  $\mu\text{m}$ ) were subsequently removed by centrifugation. Fe oxides were removed from 4  $\mu\text{m}$ -2 mm silt-sand fraction using citrate-bicarbonate-dithionite extractions and organics were removed using hydrogen peroxide (Mehra and Jackson, 1960). K-feldspar was separated from quartz using heavy liquid mixtures of bromoform and acetone. Muscovite was paramagnetically separated from biotite using a Franz magnetic separator. Exchangeable cations and cation exchange capacity measurements were made on soil and saprolite samples using unbuffered 1  $\text{NH}_4\text{Cl}$  (Huntington et al., 1990). Selected soil and saprolite samples were powdered and analyzed using X-ray fluorescence spectrometry and X-ray diffraction. Thin sections were prepared and characterized optically using an electron microprobe and scanning electron microscopy

## 3. RESULTS

### 3.1. Solid State Chemistry and Mineralogy

Average mineralogy of the fresh Panola granodiorite, determined from point counts (Table 1), indicates a preponderance of plagioclase, quartz, K-feldspar, biotite, and muscovite, with much lesser amounts of hornblende (<2%). Accessory minerals included apatite, zircon and calcite. Major mineral stoichiometries based on microprobe data are also included in Table 1. Bulk oxide data indicate strong elemental fractionations in the soils and saprolite compared to the fresh granodiorite composition (Table 2). Na and

Table 1. Mineral compositions and distributions in the unweathered Panola granodiorite. Mineral formulas based on microprobe analyses<sup>1</sup>. Weight percentages based on point counts<sup>1</sup>

Mineral	Formula	Wt % <sup>2</sup>
Quartz	SiO <sub>2</sub>	27.5
Plagioclase	Na <sub>0.77</sub> Ca <sub>0.23</sub> Al <sub>1.23</sub> Si <sub>2.77</sub> O <sub>8</sub>	31.9
K-feldspar	Na <sub>0.03</sub> K <sub>0.89</sub> Al <sub>1.02</sub> Si <sub>2.99</sub> O <sub>8</sub>	20.6
Biotite	K <sub>2.00</sub> (Mg <sub>1.78</sub> Fe(II) <sub>3.05</sub> Al <sub>0.51</sub> Ti <sub>0.30</sub> ) (Al <sub>2.40</sub> Si <sub>5.60</sub> ) O <sub>20</sub> (OH) <sub>4</sub>	12.8
Muscovite	K <sub>1.62</sub> (Mg <sub>0.28</sub> Fe(II) <sub>0.44</sub> Al <sub>1.04</sub> Ti <sub>0.10</sub> ) (Al <sub>2.94</sub> Si <sub>5.06</sub> ) O <sub>20</sub> (OH) <sub>4</sub>	7.2

<sup>1</sup> Sampled from a depth of 11.55 m at Ridge-top site

<sup>2</sup> Average analyses reported by William Kelly, NY Geological Survey

Table 2. Chemical compositions of the Panola regolith.

Sample	Depth m	Density g cm <sup>-3</sup>	SiO <sub>2</sub>	Al <sub>2</sub> O <sub>3</sub>	Fe <sub>2</sub> O <sub>3</sub>	MgO	CaO	Na <sub>2</sub> O	K <sub>2</sub> O	TiO <sub>2</sub>
			Wt%							
"A" soil	0.10	2.34	81.1	8.8	2.74	0.21	0.14	0.44	3.05	1.91
"B" soil	0.30	1.86	77.7	11.8	3.12	0.31	0.12	0.35	3.40	1.50
	0.48	1.86	64.0	19.9	5.83	0.50	0.11	0.31	2.81	1.38
	0.74	1.83	60.4	21.1	6.37	0.39	0.07	0.25	3.05	1.07
	0.84	1.73	59.9	21.7	6.76	0.44	0.06	0.23	2.63	1.21
	1.07	1.81	63.7	20.9	6.60	0.49	0.06	0.20	2.52	1.26
	1.27	1.83	60.3	22.3	6.95	0.48	0.06	0.20	2.61	1.16
	1.52	1.78	58.9	22.1	7.08	0.45	0.06	0.22	2.14	1.08
Saprolite	1.83	1.80	61.3	22.1	7.13	0.39	0.05	0.16	2.65	1.20
	2.16	1.72	61.7	23.1	6.18	0.53	0.06	0.19	3.15	1.21
	2.51	1.99	62.6	22.1	6.58	0.74	0.06	0.14	3.20	1.31
	2.84	2.25	66.0	20.6	6.05	0.81	0.07	0.23	4.41	1.33
	3.23	1.97	69.8	16.7	6.26	1.18	0.06	0.21	4.93	1.49
	3.73	2.00	65.5	21.4	5.31	1.06	0.05	0.20	4.01	1.22
	3.99	1.98	65.7	19.7	5.68	0.98	0.05	0.22	4.18	1.27
	4.29	1.92	63.6	21.0	4.80	0.90	0.05	0.23	3.06	1.00
	4.52	1.98	67.4	19.1	5.39	0.92	0.07	0.21	3.96	1.27
	4.65	2.00	69.4	18.4	5.32	1.09	0.06	0.20	4.13	1.26
4.79	1.93	60.9	18.7	4.95	1.10	0.08	0.47	5.48	1.08	
Granodiorite <sup>1</sup>	11.55	2.65	66.5	14.7	4.34	1.01	2.41	3.16	4.75	0.90

<sup>1</sup> Sample obtained from drill core described by White et al. (2001)

Ca are essentially absent in the saprolite and soil due to the near-complete weathering of plagioclase to kaolinite in the upper 6 m of the bedrock underlying the saprolite (White et al., 2001). K and Mg concentrations decrease upwards in the saprolite. Si concentrations are highest and Al and Fe concentrations are lowest in the shallow soil.

### 3.2. Weathering Characteristics

The kaolin minerals, kaolinite and halloysite, and amorphous Fe-oxyhydroxides, goethite, and hematite, are the principal secondary minerals in the soil/saprolite profile (Schroeder and Melear, 1999). In the saprolite and soil, both biotite and K-feldspar

weather to kaolinite, as evident in backscattered electron SEM images (Fig. 2). As biotite loses Fe, K, and Mg, and forms kaolinite, the mean atomic number is lowered and the image appears darker. Fig. 2A shows two "biotite grains", one of which shows the layered biotite structure becoming replaced with darker zones of kaolinite. A second, more highly weathered "biotite" grain exhibits no residual biotite, consisting of complete pseudomorphic replacement to layered kaolinite with additional box-like kaolinite structures on the grain surface. Similar epitaxial conversion of biotite to kaolinite has been observed in other saprolites (Murphy et al., 1998; Jeong, 1998; Dong et al., 1998). Biotite weathering is often initiated along cleavage planes, causing the expansion, or fanning of

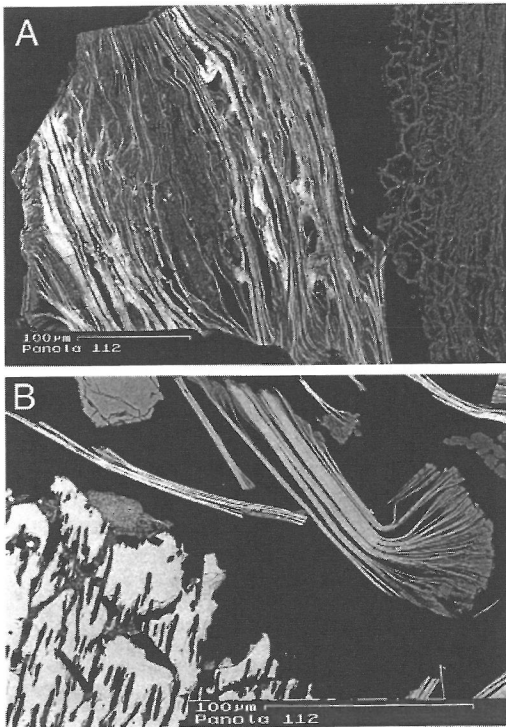


Fig. 2. SEM backscattered photomicrographs of silicate grains at a depth of 2.8 m in the Panola saprolite. (A). Left grain is partially weathered biotite. Bright segments correspond to unaltered biotite and gray areas correspond to epitaxial replacement by kaolinite. Right grain is completely kaolinized biotite with surficial box work structure. (B) Upper right biotite grain exhibits fanning and initial epitaxial replacement with kaolinite. Lower left grain is partially weathered K-feldspar with voids aligned along crystallographic axes.

the biotite grain (Fig. 2B). This morphology is described for other weathered biotites (Kretzschmar et al., 1997; Jeong, 1998; Lee and Parsons, 1999). A highly weathered K-feldspar is also included in Fig. 2B, which exhibits extensive voids and etch pits aligned along selective crystallographic planes.

Muscovite grains from the saprolite and soil appear pristine in thin section. The differences in the intensity of biotite and muscovite weathering are substantiated by compositional differences determined by microprobe analysis (Fig. 3). For single weathered "biotite" grains, the Al/Si ratios for individual dark and light interlayers range between 0.5, representative of fresh biotite, to 1.0, representative of kaolinite (Table 1). The increase in Al/Si ratios correlates with loss of K and Mg from interlayer sites due to the oxidation of octahedral Fe (Fig. 3). Similar composition ranges in epi-

taxial kaolinite-biotite are reported by Jeong (1998). Muscovites have higher Al/Si ratios than biotite, reflecting less substitution of Mg and Fe into the structure (Fig. 3). Muscovite shows no discernible trend in elemental compositions and has essentially the same compositions as in the fresh granodiorite.

### 3.3. Pore Water Hydrology

Soil porosity and gravimetric water content measurements are used to calculate hydraulic saturation of the soils and saprolite (Fig. 4A). The extent of saturation varies temporally above the saprolite/soil interface

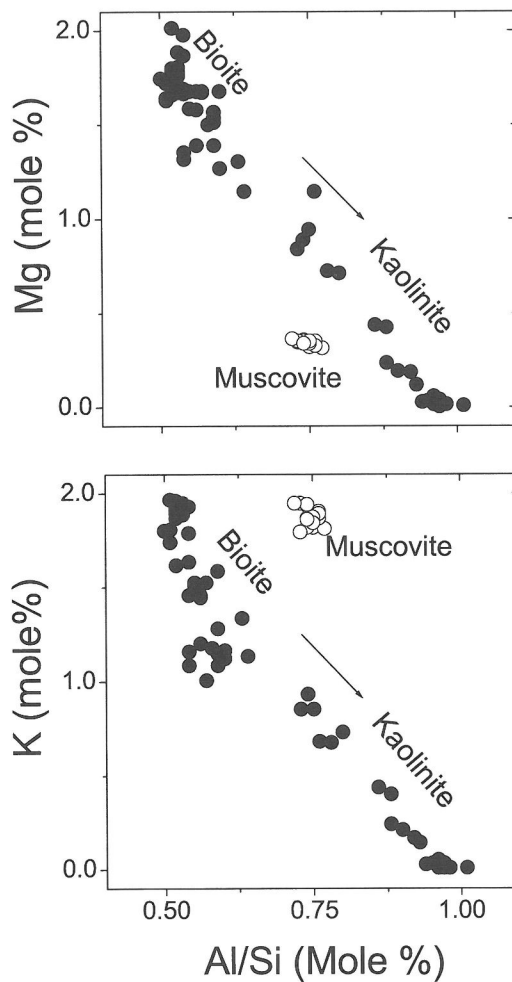


Fig. 3. Changes in Mg and K mole percentages and Al/Si ratios in biotite and muscovite as functions of regolith weathering. Arrows denote composition trends resulting from the progressive epitaxial replacement of biotite by kaolinite.

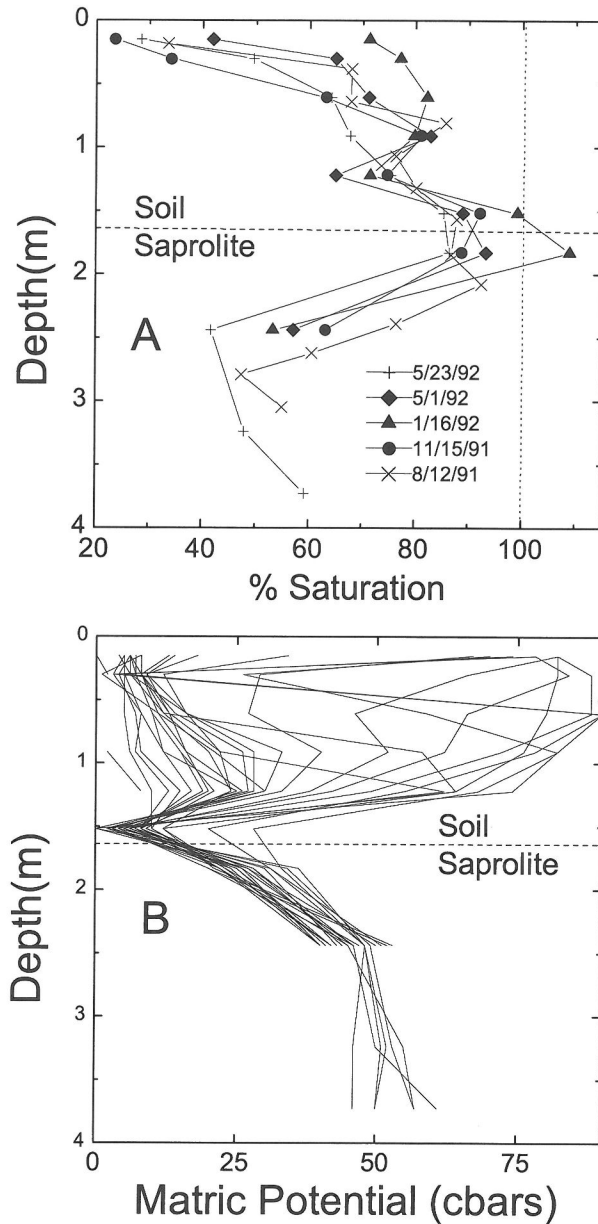


Fig. 4. Soil water hydrology of Panola ridge top. (A) Hydraulic saturation as a function of regolith depth for dates indicated. Values < 100% correspond to unsaturated conditions. (B) Soil tensions as a function of regolith depth. Lines correspond to individual samplings conducted between 8/11/91 and 10/12/93. Zero tension corresponds to hydraulic saturation and progressively higher tensions correspond to increasing undersaturation.

at 1.6 m. In the vicinity of this interface, the regolith is saturated or nearly saturated year-around. In contrast, the underlying saprolite is unsaturated. Field tensiometer readings measure capillary and adsorptive forces produced by the interaction of water with soil mineral

surfaces. Tension is zero at fully saturated conditions and increases with decreasing saturation, thus explaining the inverse relationship between saturation and tension shown in Fig. 4. In the soil zone, low moisture tensions occur from November to March (Fig. 5), cor-

responding to periods of forest dormancy and low evapotranspiration (ET) (Cappellato et al., 1993). High tensions occur during active forest growth and high ET from April to October. Superimposed on this seasonal trend in shallow soil tensions are specific precipitation events such as the intense June 1992 storms shown in the precipitation record in Fig. 5. These events temporarily decreased the matric potential, even during seasonally high rates of transpiration. Moisture tensions below 1.6 m in the saprolite were essentially unaffected by these storm events or longer term seasonal trends in ET.

The soil/saprolite interface (1.6 m) is a zone of consistent pore water saturation and near-zero matric potentials (Fig. 4). These conditions are indicative of "perched water" which overlays a low-permeability duripan consisting of a 10-cm thick layer of relatively competent clay. Duripans serve as aquitards, which restrict the downward percolation of water. Duripans at soil/saprolite boundaries are commonly observed in the southeastern Piedmont of the U.S.A. (Simpson, 1986; Buol and Weed, 1991). From observations in thin sections, O'Brien and Buol (1984) concluded that low hydraulic conductivity is related to the absence of continuous pores due to the formation of thick cutans of clay translocated from the overlying soil. While cyclic wetting and drying occurs in the overlying soil horizons, the underlying saprolite maintains nearly constant moisture contents that are dampened to responses to individual storm events and longer-term trends in seasonal ET (Fig. 5).

### 3.4. Pore Water Chemistry

Representative pore water solutes obtained from the suction water samplers in soil and saprolite are tabulated in Table 3. Also included are data for open fall and through fall precipitation, surface water, and ground water. Na and Cl are moderately concentrated relative to average precipitation above the duripan and strongly concentrated below the duripan (Fig. 6). The shallow solutes reflect the direct influences of seasonal ET, which concentrates Na and Cl due to selective exclusion by vegetation. Perched water directly above the duripan undergoes significantly greater ET due to longer residence times. Subsequent slow leakage of this water into the upper saprolite explains the high Na and Cl concentrations. This effect may also be exaggerated by sampling bias. During dry periods, the air entry potentials for the porous cup samplers in the shallow soils become very high compared to the potentials in the wetter saprolite (Fig. 4B), thus preventing the sampling of highly evaporated waters. Na/Cl ratios are similar to precipitation (Table 3). The granodiorite is essentially devoid of Cl, and Na, which is associated primarily with plagioclase, is effectively weathered from the underlying bedrock (White et al., 2001).

Solute Si, directly below the duripan, is less concentrated than Na and Cl, suggesting non-conservative behavior related to the incorporation of Si into ongoing kaolinite formation in the duripan. Si increases in the deeper saprolite, particularly near the bedrock interface, thus indicating silicate weathering. Pore water Ca, Mg, and K concentrations exhibit sig-

Table 3. Representative chemical concentrations of pore water, precipitation, stream water, and ground water in Panola watershed ( $\mu\text{mole}\cdot\text{l}^{-1}$ ).

	Pore Waters <sup>1</sup>					Wet <sup>2</sup> Precip.	Thru <sup>3</sup> Fall	Surface <sup>4</sup> Water	Ground <sup>5</sup> Water
Depth	0.30	0.91	1.83	3.00	4.62	na	na	na	2.5
pH	5.80	5.54	5.39	5.37	5.58	4.83	4.05	5.09	5.25
Na	24.3	40.0	202	206	163	11.4	10.6	42.1	117.2
K	41.0	36.2	43.7	17.7	12.9	1.8	10.6	8.7	14.5
Ca	55.9	25.5	24.1	12.5	14.5	3.3	32.0	18.4	17.2
Mg	30.4	81.7	66.5	56.4	35.2	1.7	19.2	12.1	19.0
Al	4.6	4.0	0.9	2.3	4.7	na	na	9.5	3.4
SiO <sub>2</sub>	75.1	92.9	201	189	372	na	na	76.8	182.2
Alk	86.9	63.4	30.8	25.4	55.6	0.0	0.0	0.0	59.4
Cl	27.6	34.1	251	319	174	14.1	20.6	30.2	67.3
NO <sub>3</sub>	1.4	1.1	23.8	2.8	2.1	31.6	19.3	0.0	0.7
SO <sub>4</sub>	47.9	43.9	10.3	1.6	6.1	36.8	42.7	51.0	36.5

<sup>1</sup>Sampled 1/21/93

<sup>2</sup>Average of precipitation events 2/82 -7/88

<sup>3</sup>Cappellato et al., 1993

<sup>4</sup>Upper gauge, sampled 1/23/93

<sup>5</sup>Well 700 sampled 1/23/93

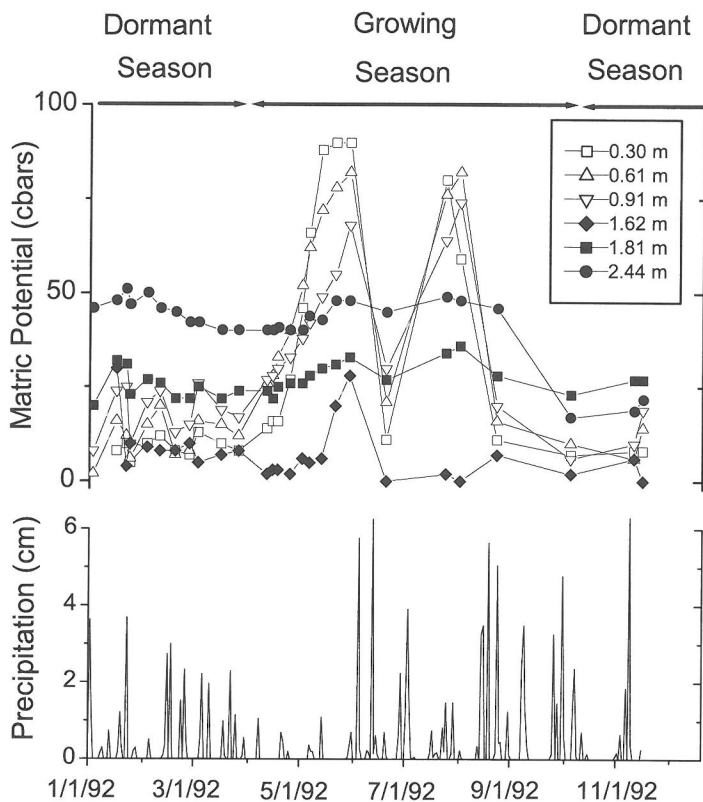


Fig. 5. Seasonal variations in soil tensions and precipitation events for 1992. Also indicated are the approximate periods of forest growth and dormancy. (dates: mo/day/yr)

nificantly greater seasonal variability in the soil than do Na, Cl, and Si. This indicates that, in addition to the effects of ET, these elements are being selectively added and/or removed by biologic cycling by throughfall, leaf fall, and root uptake. In the underlying saprolite, Ca, Mg, and K concentrations are consistently lower than in the soils. The lack of concurrent cation increases along with Si indicates that silicate weathering is not the dominant control on solute Ca, Mg and K in the saprolite.

### 3.5. Mineral Surface Areas

Bulk regolith BET surface areas increase with increasing depth in the lower soil and upper saprolite (Table 4 and Fig. 7A), corresponding to increasing Al and Fe concentrations and more abundant kaolinite and Fe-oxides (Table 2). These phases decrease in the underlying saprolite, thus accounting for a decrease in bulk BET surface areas. Specific mineral surface areas are also tabulated in Table 4 and plotted versus

depth in Fig. 7B. Kaolinite surface areas range between 11.1 and 28.5  $\text{m}^2 \text{g}^{-1}$ , which correspond to a reported range for kaolinite (6 to 39  $\text{m}^2 \text{g}^{-1}$ ; Dixon and Weed, 1977). Fe-oxide surface areas calculated from the difference in bulk surface area before and after dithionite extraction range from 10.7 to 38.3  $\text{m}^2 \text{g}^{-1}$  and approach values reported for goethite (32 to 71  $\text{m}^2 \text{g}^{-1}$ ; Buffle, 1988).

The weathered primary silicates exhibit significantly lower specific surface areas than do the secondary clay and Fe oxyhydroxides (Table 4 and Fig. 7B). Mean average silicate grain sizes varied between 0.27 to 0.54  $\mu\text{m}$  with depth in the regolith. Biotite surface areas range between 1.25 and 7.2  $\text{m}^2 \text{g}^{-1}$ , which is similar to that reported for epitaxially-weathered biotites in saprolites in Puerto Rico (Murphy et al., 1998). These values are much higher than surface areas of fresh biotite (0.24  $\text{m}^2 \text{g}^{-1}$ ; Acker and Bricker, 1992) and, in part, reflect the kaolinite intergrowths replacing biotite (Fig. 2A). The K-feldspar surface areas are also high (2.3 to 8.1  $\text{m}^2 \text{g}^{-1}$ ) and may reflect interstitial

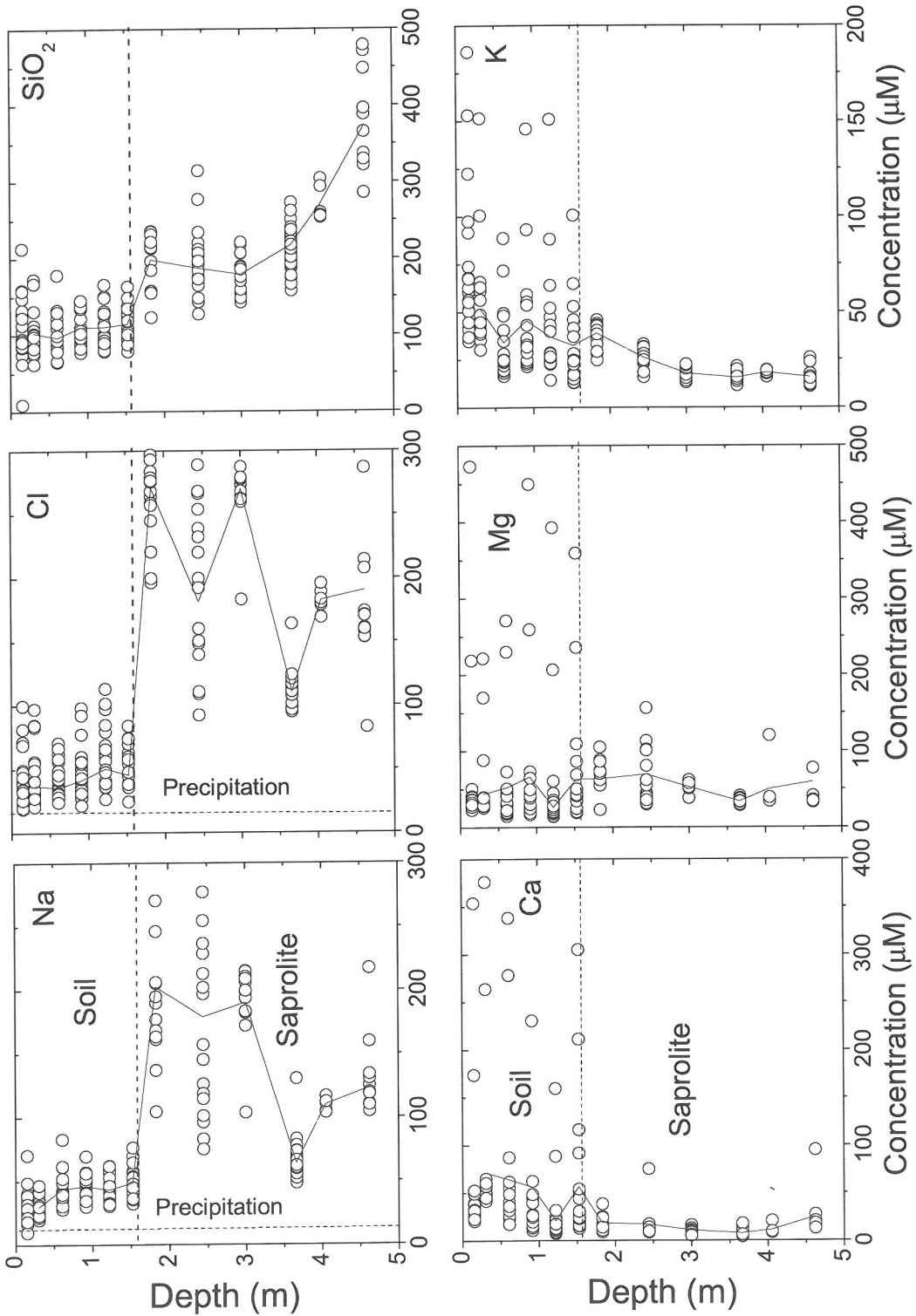


Fig. 6. Pore water solute concentrations with depth in the regolith. Samples collected between 12/91 and 4/93. Vertical dashed lines show average concentrations in open fall precipitation.

Table 4. Surface areas of regolith and specific minerals with depth ( $\text{m}^2\cdot\text{g}^{-1}$ ).

Depth m	Bulk Regolith	Kaolinite	Fe-oxide	Qtz	Biotite	K-spar
0.10	2.68	12.9	nd	0.15	nd	2.35
0.20	3.56	11.0	10.7	0.18	nd	4.65
0.38	13.5	20.5	12.6	0.14	1.70	4.64
0.48	20.3	26.7	12.5	0.19	1.25	3.83
0.56	21.4	28.5	43.1	0.20	1.64	3.61
0.74	12.8	15.6	41.7	nd	nd	nd
0.84	16.3	11.1	38.3	0.16	1.47	4.41
1.52	17.9	15.6	22.4	0.11	4.62	8.20
1.83	14.2	11.0	22.2	0.11	2.88	7.10
2.84	7.78	12.6	26.5	nd	nd	nd
3.23	5.64	11.8	32.4	0.22	4.43	1.72
3.53	4.90	13.3	10.9	0.42	7.19	7.23
3.99	7.33	23.3	11.8	0.27	6.58	8.13
4.29	8.28	12.8	11.2	0.23	6.76	nd
4.52	8.10	12.1	16.4	0.24	4.09	nd

nd = not determined.

Table 5. Exchangeable cation concentrations ( $\text{mM kg}^{-1}$ ) and cation exchange capacities (CEC) in  $\text{mEq kg}^{-1}$ 

Depth	Na	K	Mg	Ca	Al	CEC
0.05	0.25	0.91	0.70	2.35	1.77	12.6
0.15	0.09	0.88	0.88	2.82	1.11	11.7
0.25	0.30	1.80	1.55	3.67	2.65	20.5
0.34	0.23	2.59	2.39	5.73	2.26	25.8
0.46	0.38	3.01	4.68	8.36	1.48	33.9
0.52	0.44	2.66	5.09	7.27	3.13	37.2
0.61	0.63	3.15	4.00	4.17	8.52	45.7
0.70	0.53	2.27	4.42	3.30	7.43	40.5
0.79	0.56	2.04	4.09	2.15	8.06	39.3
0.88	0.56	2.16	3.91	1.35	22.36	80.3
1.03	0.54	2.51	3.00	0.71	17.56	63.1
1.22	0.29	2.29	2.27	0.26	5.50	24.1
1.49	0.24	2.15	1.35	0.07	5.56	21.9
1.78	0.12	1.71	1.18	0.06	5.54	20.9
2.11	0.34	1.89	1.13	0.10	8.87	31.3
2.46	0.13	0.51	1.13	0.03	6.09	21.2
2.78	0.21	0.84	0.89	0.09	22.66	71.0
3.16	0.33	0.99	0.82	0.05	14.44	46.4
3.47	0.21	0.75	0.92	0.03	2.63	10.7
3.58	0.26	0.90	1.03	0.06	3.01	12.4
3.68	0.56	1.33	1.08	0.06	9.90	33.9
3.86	0.50	0.84	1.75	0.05	47.83	148
4.05	0.33	0.85	1.98	0.19	53.53	166
4.20	0.25	0.78	2.08	0.18	83.93	257
4.34	0.19	0.57	1.67	0.19	33.45	105
4.46	0.24	0.74	1.14	0.22	39.25	121
4.58	0.25	0.72	0.93	0.20	17.38	55.4

kaolinite. Quartz has the lowest specific surface areas in the regolith ( $0.11$  to  $0.42 \text{ m}^2 \text{ g}^{-1}$ ), which is consistent with weathered quartz surface areas reported elsewhere ( $0.10$  to  $0.23 \text{ m}^2 \text{ g}^{-1}$ , White et al., 1996;  $0.15$  to  $0.40 \text{ m}^2 \text{ g}^{-1}$ , Schulz and White, 1999).

The contributions of specific minerals to the bulk regolith surface areas are calculated based on the wt % of each mineral present (Fig. 7C). At the shallowest soil depths, almost all of the bulk surface area is attributed to kaolinite. With increasing soil depth, Fe-hydroxides contribute equally to the bulk surface areas. In the underlying saprolite, increasing percentages of primary minerals dominate the bulk surface area. The line plotted on the far right of Fig. 7C is the sum of the surface areas contributed by the individual minerals. These calculated percentages are only slightly higher than the bulk regolith surface area (100%), implying that the removal of secondary minerals by chemical extraction and sonification does not expose significant additional primary mineral surface areas.

### 3.6. Cation Exchange

Except in the shallowest soil horizons, Al is the dominant cation produced by  $\text{NH}_4\text{Cl}$  extraction (Table 5 and Fig. 8A). Maximum extractable base cations occur between  $0.5$  and  $1.0 \text{ m}$  in the soil; Ca dominates, with lesser amounts of Mg and K, and very low concentrations of Na (Fig. 8B). In the deeper soil ( $>1.0 \text{ m}$ ) and in the underlying saprolites, base cations are significantly less abundant, with higher proportions of Mg and K that reflect the diminished role of biological cycling and increased effects of weathering of biotite and K-feldspar.

Cation exchange occurs principally on secondary kaolinite and Fe-oxides in the Panola regolith. Cation exchange also occurs with soil organic matter at shallower depths. The average cation exchange capacity (CEC) for Piedmont kaolinite is  $40 \text{ meq kg}^{-1}$  (Jardine

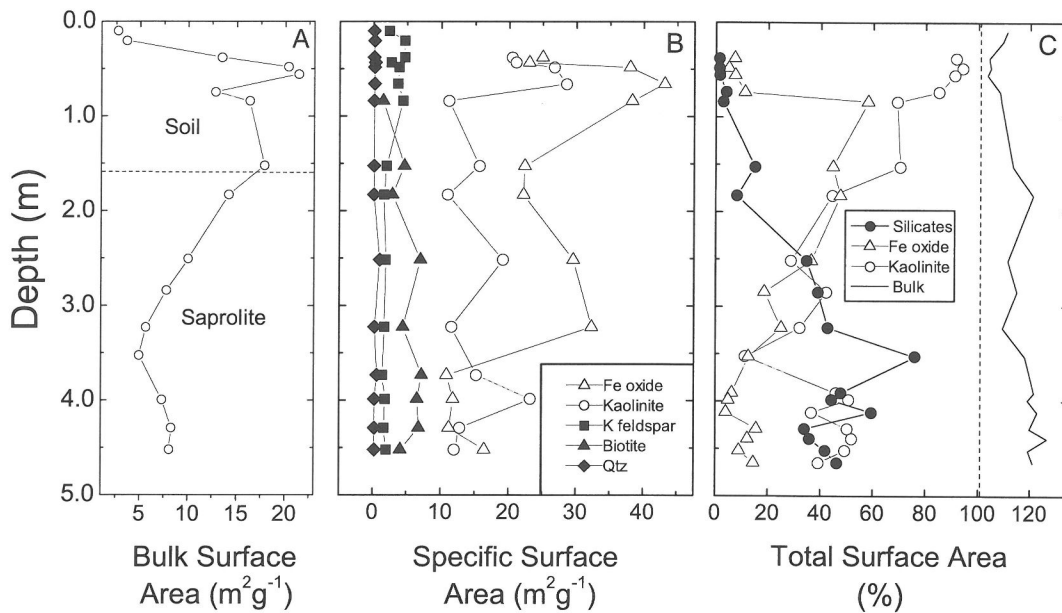


Fig. 7. Surface areas versus regolith depth. (A) Bulk surface areas. (B) Specific mineral surface areas. Solid points are primary minerals and open points are secondary minerals. (C) Percent contribution of specific mineral surface areas to total surface areas. Line on right side of plot is the total percentage contributed by individual minerals compared to bulk surface area (dashed vertical line = 100%).

et al., 1985; Levy et al., 1988; St. Pierre et al., 1992) and the average CEC for goethite is 100 meq kg<sup>-1</sup> (Al-Kanani and MacKenzie, 1990). The expected CEC for the Panola regolith is calculated based on these average CEC values and wt % kaolinite and goethite present in the Panola regolith. This distribution with depth is then compared to the measured total CEC (Fig. 8D). Kaolinite and Fe-oxide concentrations are low in the shallowest soils (<0.5 m) due to translocation and dissolution by high concentrations of organic acids (Fig. 8C). Consequently, the total cation exchange capacity is low (Fig. 8D). These phases reach maximum concentrations between 0.5 to 1.0 m in the soil, which correspond to the zone of maximum base cation exchange (Fig. 8B). Decreases in the proportions of kaolinite and Fe-oxhydroxides in underlying saprolite correlate with increases in primary silicates and decreases in base cation exchange.

Base cation saturation (BS), defined as the ratio of sum of exchangeable base cations to the sum of total cations, including Al (Driscoll et al., 1985), ranges from between 85% in the shallow soil to 2% in horizons with very high extractable Al concentrations at depths of 0.8, 2.8, and 4.2 m (Fig. 8D). Unlike for base cations, these Al "spikes" do not correspond to

kaolinite and goethite increases in the regolith (Fig. 8C). The discrepancy between calculated and measured CECs (Fig. 8D) implies that only a small portion of extractable Al reflects true cation exchange, with the remainder derived from dissolution of a readily soluble aluminum phase (Shanley, 1992). The highest extractable Al occurs near the saprolite/bedrock interface, suggesting that readily soluble Al-containing phases, such as amorphous Al hydroxides or allophane, are forming as the result of extensive K-feldspar weathering at this interface.

#### 4. DISCUSSION

The mineralogical changes and elemental mobility observed in the Panola regolith have resulted principally from long-term fluid flow through the regolith. Solute transport must supply reactants, principally carbonic acid, and organic acids in the shallower soil horizons, that promote weathering reactions. In turn, solute transport is responsible for removing reaction products from the weathering environment. It is this latter transport which forms the basis for evaluating current weathering rates in the Panola regolith, and permits comparison with past long-term rates based on elemental and mineralogical changes.

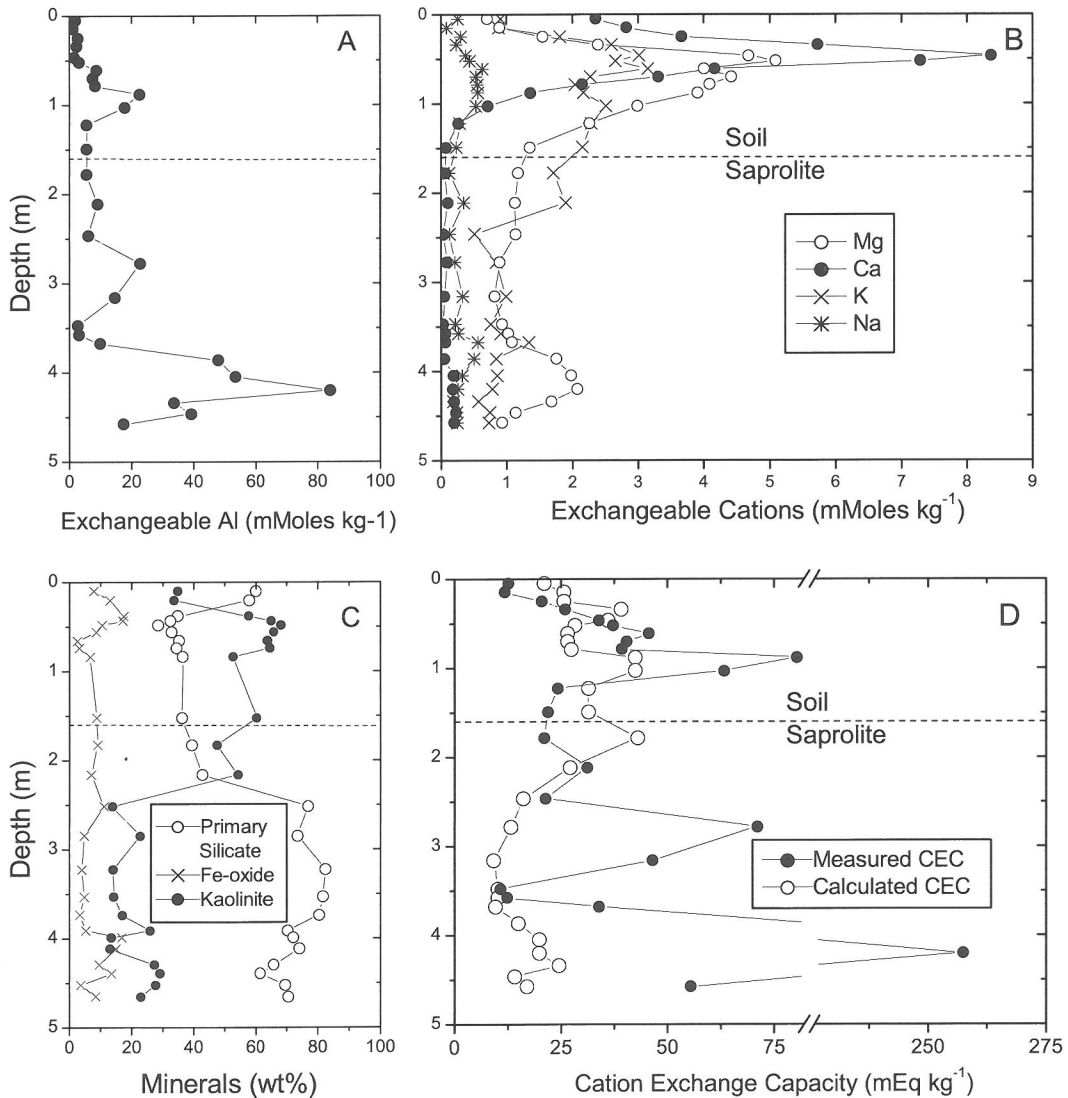


Fig. 8. Cation exchange versus regolith depth. (A) Exchangeable Al. (B) Exchangeable base cations. (C) Wt % of primary silicates and secondary minerals. (D) Comparison of measured cation exchange capacities (solid circles) and calculated CEC based on percentage of mineral phases present.

#### 4.1. Characterization of Solid State Mobility

The data presented in the preceding sections are sufficient to construct mass balances describing element mobility in the Panola saprolite (White et al., 2001). Briefly, quantitative gains or losses of an element or mineral  $j$ , due to weathering, can be obtained from the regolith concentration  $C_{j,w}$  ratioed against the concentration  $C_{j,p}$  in the underlying unweathered protolith. This ratio  $C_{j,w}/C_{j,p}$  is dependent on three parameters as defined in Eqn. 1 (Brimhall and Dietrich, 1987)

$$\frac{C_{j,w}}{C_{j,p}} = \frac{\rho_p}{\rho_w} \frac{I}{(\epsilon_i + 1)} (1 + \tau_j) \quad (1)$$

The ratio of the density of the protolith to regolith,  $\rho_p/\rho_w$ , is associated with the dissolution and precipitation of mobile elements. The volume ratio  $V_w/V_p$ , resulting from soil compaction or expansion, determined for a conservative chemical species  $i$ , is described by the strain factor  $I/(\epsilon_i + 1)$ , where  $\epsilon_i = V_w/V_p - 1$ . Together, density and volume changes describe closed-system contributions, which occur

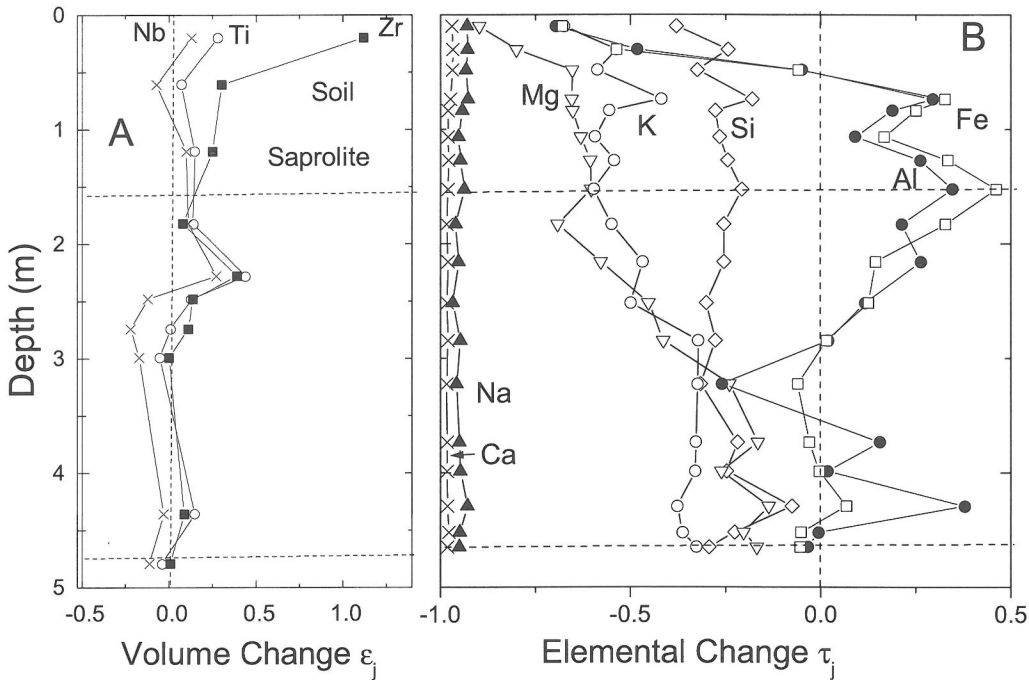


Fig. 9. Volume changes and elemental mass transfers within the Panola regolith. (A) Volumetric compaction and dilation are denoted by values of  $\epsilon_j < 0$  and  $\epsilon_j > 0$ , respectively. A value of  $\epsilon_j = 0$  denotes isovolumetric weathering. (B) Elemental changes with regolith depth. A value  $\tau_j = 0$  denotes no elemental loss,  $\tau_j = -1$  indicates complete elemental loss, and  $\tau_j > 1$  denotes elemental additions.

without movement of the component under consideration. The mass transfer coefficient  $\tau_j$  is an open-system contribution that describes mobility of component  $j$  across a unit volume of regolith.

The density ratios  $\rho_p/\rho_w$  in Eqn. 1 are calculated directly from the bulk density measurements in the weathered regolith and an assumed granodiorite density of  $2.6 \text{ g cm}^{-3}$ . The volumetric strain can then be determined from the ratios of densities and concentrations of an inert element  $i$  in the soil and protolith (Eqn. 1) to give

$$\epsilon_i = \frac{\rho_p C_{i,p}}{\rho_w C_{i,w}} - 1 \quad (2)$$

Positive values of  $\epsilon_i$  indicate expansion of the regolith and negative values indicate collapse. A value of  $\epsilon_i \approx 0$  is indicative of isovolumetric weathering.

The extent of volumetric changes in the regolith is best established by considering a suite of inert elements. Except for the shallowest soils, which may have undergone volume increases due to bioturbation and the introduction of organic matter,  $\epsilon_i$  values calculated from Zr, Ti, and Nb soil concentrations center close to zero (Fig. 9A), indicating that weathering is essentially iso-volumetric. Isovolumetric weathering is commonly

observed for saprolites developed on granites and gneisses in the Piedmont of southeastern United States (Cleaves, 1993; Markewich and Pavich, 1991).

Elemental mobility during regolith weathering is characterized by the mass transfer coefficient  $\tau_j$  (Eqn. 1), which is computed from density and chemical composition data in combination with volume change derived from the strain calculations.

$$\tau_j = \frac{\rho_w C_{j,w}}{\rho_p C_{j,p}} (\epsilon_i + 1) - 1 \quad (3)$$

The following calculations assume that Ti is conservative. When  $\tau_j = -1$ , element  $j$  is completely removed during weathering. If  $\tau_j = 0$ , the element is immobile during weathering with respect to the volume of regolith considered.

Ca and Na are almost completely mobilized in the saprolite and soil relative to the fresh bedrock (Fig. 9B,  $\tau_{\text{Na,Ca}} \approx -1$ ). This is attributed to near-complete weathering of plagioclase to kaolinite in the upper Panola bedrock (White et al., 2001). The significant losses of K ( $\tau_K = -0.33$ ) and Si ( $\tau_{\text{Si}} = -0.29$ ) at the bedrock/saprolite interface correspond to extensive K-feldspar weathering (Fig. 9B). Mg loss, attributed to biotite weathering at this interface, is less ( $\tau_{\text{Mg}} =$

-0.16). Mg decreases more rapidly than K upwards in the saprolite and is strongly depleted in the soil A horizon ( $\tau_{Mg} = -0.89$ ). Fe and Al are also strongly depleted in the upper A soil horizon ( $\tau_{Fe} = -0.67$  and  $\tau_{Al} = -0.70$  at 0.1 m), but are significantly enriched relative to fresh bedrock concentrations in the underlying B-horizon and in the upper saprolite ( $\tau_{Fe} = +0.45$  and  $\tau_{Al} = +0.30$  at 1.6 m). This distribution is indicative of downward Fe and Al mobilization and subsequent re-precipitation as goethite and kaolinite.

The elemental loss or gain  $\Delta M_j$  (moles) in the saprolite and soil, normalized to unit regolith surface area ( $m^2$ ), are calculated from the expression (Chadwick et al., 1990; White et al., 2001):

$$\Delta M_{j,l} = \left( \rho_p \frac{C_{j,p}}{w_j} \times 10^4 \right) \int_{Z=d_1}^{Z=d_2} -(\tau_{j,s}) dZ \quad (4)$$

in which an interval of regolith thickness is defined as  $\Delta Z$  (m),  $\rho_p$  is density ( $cm^{-3}$ ), and  $w_j$  is the atomic weight of element  $j$ . Table 6 indicates that significantly more K than Mg is lost during the conversion of bedrock to saprolite, but that on a percentage basis the losses of K and Mg are comparable. These base cations are effectively removed from the regolith through solute transport. Si is partly removed from the regolith, with the remainder re-precipitated as kaolinite. Although Fe and Al are mobilized in the upper soil zone (Table 6), their total percentages in the total thickness of regolith increase slightly relative to the protolith due to re-precipitation of Fe and Al as Fe-oxyhydroxides in the lower soil and saprolite (Fig. 9).

#### 4.2. Characterization of Solute Fluxes

The mass loss  $\Delta m_j$  (moles) of an element  $j$  from the regolith is related to the rate of pore water movement through a unit surface area of regolith ( $m^2$ ) by the expression (White et al., 1996):

$$\Delta m_j = 1000 \Delta c_j q_h t \quad (5)$$

where  $\Delta c_j$  is the change in the molar aqueous concentration and  $t$  is time (s). The fluid flux density  $q_h$

( $m s^{-1}$ ), which is the rate of fluid transported over unit area in Eqn. 5, is given by

$$q_h = -K \nabla H \quad (6)$$

where  $K$  is the hydraulic conductivity and  $\nabla H$  is the hydraulic gradient. For unsaturated flow, which dominates in the Panola regolith,  $\nabla H$  is also dependent on variations in regolith saturation. The change in head with depth can be described such that (Hillel, 1982)

$$\frac{dH}{dz} = \frac{dh_g}{dz} + \frac{dh_p}{dz} \quad (7)$$

where  $h_g$  is the gravitational head at any point and  $h_p$  is the head related to the matric potential of the soil mineral surfaces. Determinations of fluid, and conversely chemical fluxes, based on Eqns. 6 and 7, are difficult for most unsaturated conditions due to the non-linear dependence of conductivity and head potentials on moisture content. Special cases for Eqns. 6 and 7 are discussed by Stonestrom et al. (1998) in which constant matric potentials or tensions exist within a vertical section of a weathering regolith (i.e.,  $dh_p/dz = 0$ ).

The duripan at the soil/saprolite interface in the Panola regolith produces a unique hydrology conducive to estimating unsaturated flow in the underlying saprolite. Although LiBr tracer studies have demonstrated significant ET and lateral flow off the ridge top above the duripan (Huntington et al., 1994), negligible lateral flow is assumed to occur in the saprolite beneath the duripan. If evapotranspiration is minor at depth, the mass of water can be assumed to be conservative and the unsaturated flux density  $q_h$ , due to drainage anywhere in the saprolite, will approximate the saturated flux density in the overlying duripan. Under saturated conditions  $h_p = 0$  and  $dh_g/dz = -1$  (Eqn. 7). The flux density is approximated as the inverse of the saturated hydraulic conductivity

$$q_h = -K_{sat} \quad (8)$$

The solute transported in the unsaturated saprolite can be directly calculated if the saturated hydraulic conductivity of the duripan is known.

#### 4.3. Estimates of Fluid Fluxes and Residence Times

Saturated hydraulic conductivities  $K_{sat}$  ( $m s^{-1}$ ) measured on core material, inclusive of the duripan (0.78 to 2.35 m), vary between  $1.3 \times 10^{-9}$  to  $5.0 \times 10^{-6}$   $m s^{-1}$  (Table 7 and Fig 10). These conductances are comparable to those measured in soil/saprolites elsewhere in the southeastern United States (Vapraskas and Williams, 1995; Schoenberger et al., 1995). A minimum conductivity of  $K_{sat} = 1.3 \times 10^{-9}$   $m s^{-1}$  corresponds to an infiltration rate of  $4.1 \times 10^{-2}$   $m yr^{-1}$  in the

Table 6. Elemental mobilities (moles  $m^{-3}$ ) and % total loss in the Panola regolith.

	Saprolite	Soil	% loss
Depth	1.2 - 4.7 m	0.0 - 1.6 m	
Si	-5520	-160	22.7
K	3360	120	43.1
Mg	630	-20	43.8
Fe	-120	540	-8.9
Al	-2030	1780	-10.7
Na	670	-90	94.6
Ca	40	-14	97.9

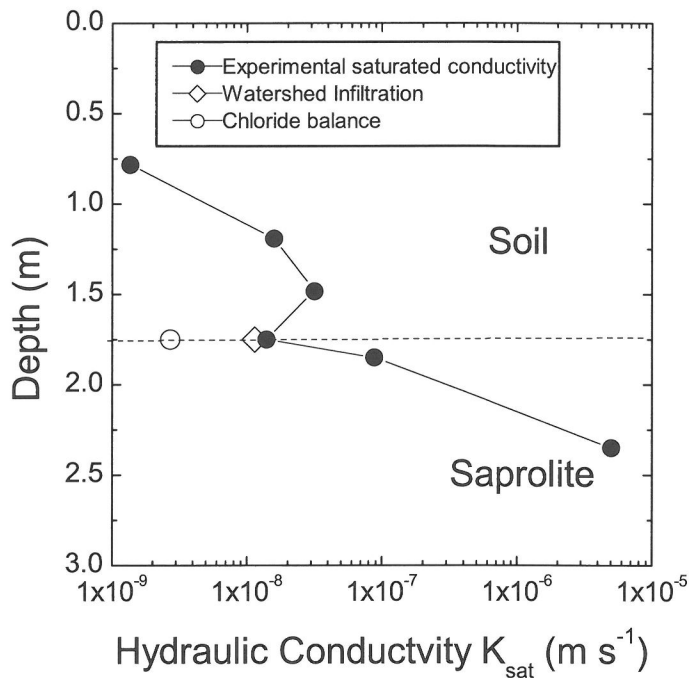


Fig. 10. Laboratory-determined saturated hydraulic conductivities for the soil and saprolite. Also included are estimated infiltration rates based on Cl mass and watershed water balances.

shallow soil (Fig. 10). This rate is clearly contradicted by rapid soil moisture and tension responses to precipitation events (Figs. 4 and 5). Water movement in the shallow soil at Panola occurs as macropore flow, principally along root channels and worm borrows (Flury and Fluhler, 1994). This macropore flow short-circuits the much slower matrix flow measured in the small-scale hydraulic conductivity experiments presented in the present study.

Deeper in the regolith, isovolumetric conditions (Fig. 9A) denote a lack of extensive bioturbation and macropore flow. The measured  $K_{sat}$  in the duripan is  $1.4 \times 10^{-8} m s^{-1}$  or  $0.44 m yr^{-1}$  (Fig. 10). This low permeability is responsible for near-saturated to saturated conditions which prevail at the soil/saprolite interface. Due to increased porosity, higher saturated conductivities occur in the saprolite directly beneath the duripan. A maximum value of  $K_{sat} = 5.0 \times 10^{-6} m s^{-1}$  at 2.35 m (Table 7) corresponds to an infiltration rate of  $>150 m yr^{-1}$ , thus explaining the lack of saturated conditions in the saprolite (Fig. 4A). Unsaturated conductivities  $K_{unsat}$  decrease exponentially with decreases in regolith water content (Stonstrom et al., 1998). Therefore,  $K_{unsat}$  can be several orders of magnitude lower

than  $K_{sat}$ . In the Panola regolith, the assumption of water conservation beneath the soil horizon requires that unsaturated flow in the saprolite must equal saturated infiltration through the overlying duripan.

Experimental conductivities (Table 7) can be compared against independent estimates for field infiltration. Average precipitation  $P$  in the Panola watershed is  $1.15 m yr^{-1}$  and average runoff, normalized to watershed surface area, is  $0.34 m yr^{-1}$  (Huntington et al., 1993). The resultant water loss due to ET is 71%. Assuming that the remaining runoff infiltrates through the saprolite, the resulting conductivity for the watershed would be  $1.2 \times 10^{-8} m s^{-1}$ , which is essentially identical to the experimental hydraulic conductivity for the duripan ( $1.4 \times 10^{-8} m s^{-1}$ ). This is a maximum estimate for the fluid flux because negligible lateral flow is assumed to occur above the saprolite.

An additional method for estimating field flux density is based on ET-corrected precipitation using Cl as a conservative tracer (Eriksson and Kunakasen, 1969)

$$q_h = P (Cl_p / Cl_s) \quad (9)$$

where  $Cl_p$  and  $Cl_s$  are the respective Cl concentrations in precipitation and in the pore water. Average

Table 7. Saturated hydraulic conductivities in Panola and comparable regoliths.

	Depth (cm)	$K_{sat}$ ( $m\ s^{-1}$ )
<b>Granodiorite, Panola, Georgia, USA<sup>1</sup></b>		
B horizon	0.78	$1.34 \times 10^{-9}$
B horizon	1.19	$1.58 \times 10^{-8}$
B horizon	1.48	$3.16 \times 10^{-8}$
B horizon	1.75	$1.39 \times 10^{-8}$
B/Saprolite	1.85	$8.84 \times 10^{-8}$
Saprolite	2.35	$5.08 \times 10^{-6}$
<b>Quartz Diorite, North Carolina, USA<sup>2</sup></b>		
Saprolite	2.0	$1.03 \times 10^{-7}$
<b>Felsic Gneiss, North Carolina, USA<sup>3</sup></b>		
B horizon	0.28	$1.62 \times 10^{-6}$
B/Saprolite	0.6	$7.00 \times 10^{-8}$
Saprolite	1.87	$8.10 \times 10^{-7}$
<b>Quartz Diorite, Luquillo Mtns., PR<sup>4</sup></b>		
Saprolite	0.68	$5.5 \times 10^{-6}$

<sup>1</sup> This study, <sup>2</sup>Vapraskas & Williams (1995),

<sup>3</sup> Schoenberger et al., 1995, <sup>4</sup>White et al. (1998).

Cl in precipitation is  $14\ \mu\text{M}$  (Table 3) and average pore water Cl in the saprolite is  $200\ \mu\text{M}$  (Fig. 6). The resultant flux density is  $2.6 \times 10^{-9}\ \text{m}\ \text{s}^{-1}$ , or about a factor of 6 less than the saturated conductivity  $K_{sat}$  of the duripan ( $1.4 \times 10^{-8}\ \text{m}\ \text{s}^{-1}$ ).

The residence time of pore water in the saprolite can be calculated from the relationship

$$t_r = \frac{\phi s d}{q_h} \quad (10)$$

where  $\phi$  is the average saprolite porosity (0.45),  $s$  is the average fractional saturation (0.7), and  $d$  is the saprolite thickness (3.0 m). The average pore water residence time is  $3.6 \times 10^8\ \text{s}$  (12 years), based on the minimum Cl-derived flux density ( $2.6 \times 10^{-9}\ \text{m}\ \text{s}^{-1}$ ). These residence times are long when compared to hill slope waters which have been age-dated in the watershed (Burns et al., 1998). Unlike the hillslope flow, which responds rapidly to individual storm events through macropore flow, the deeper ridge-top saprolites are much less responsive to individual or even longer-term season patterns in precipitation and ET (Fig. 5).

#### 4.4. Comparison of Short- and Long-Term Rates of Silica Weathering

Of the major elements associated with silicate weathering, only Si exhibits consistent pore water increases with depth in the saprolite (Fig. 6). Assuming that the present short-term weathering flux  $r_{Si}$  (moles  $\text{m}^{-2}\ \text{s}^{-1}$ ) is comparable to past long-term weathering flux  $R_{Si}$  (moles  $\text{m}^{-2}\ \text{s}^{-1}$ ), the relationship can be developed

$$r_{Si} = \frac{\Delta m_{Si}}{t} = \frac{\Delta M_{Si}}{t^*} = R_{Si} \quad (11)$$

where  $\Delta m_{Si}$  (Eqn. 5) is the Si loss over the fluid residence time  $t$  (s) and  $\Delta M_{Si}$  (Eqn. 4) is the solid-state Si loss over the duration of saprolite weathering ( $t^*$ ). The maximum pore water residence time is 12.6 yrs (Eqn. 10) and the average increase in pore water Si in the saprolite is  $\Delta c_{Si} = 255\ \mu\text{M}$  (Fig. 6). Therefore the present day Si flux  $r_{Si}$  (Eqn. 11) is  $2.0 \times 10^{-2}$  moles  $\text{m}^{-2}\ \text{yr}^{-1}$ .

Bierman et al. (1995) measured  $^{36}\text{Cl}$  concentrations in surface outcrops of granodiorite within the Panola watershed and calculated exposure ages of between 250–500 kyrs. These distributions produced a mean model erosion rate of  $7\ \text{m}\ \text{my}^{-1}$ , which is in agreement with steady-state chemical weathering rates calculated from solute fluxes. The time span required to produce 3 m of saprolite is estimated to be  $4.3 \times 10^5$  yrs. The long term Si loss is  $\Delta M_{Si} = 5.5 \times 10^3$  moles (Eqn. 4 and Table 6). The resulting long-term Si flux is  $R_{Si} = 1.3 \times 10^{-2}$  moles  $\text{m}^{-2}\ \text{yr}^{-1}$  (Eqn. 11), which is similar to the present day rates based on Cl balances ( $r_{Si} = 2.0 \times 10^{-2}$  moles  $\text{m}^{-2}\ \text{yr}^{-1}$ ).

The effect of infiltration rates on estimates for solute weathering is emphasized by plotting weathering trajectories (White et al., 1998). The mass loss  $\Delta M_{Si}$  resulting from long-term regolith weathering is plotted in Fig. 11. The upward trending lines are weathering trajectories calculated by the extrapolation of solute loss  $\Delta m_{Si}$  to long times based on Eqn. 5 and various rates of infiltration. Sustained saturated flow in the saprolite replicates total Si loss in less than  $2 \times 10^3$  years, an unreasonable time span.

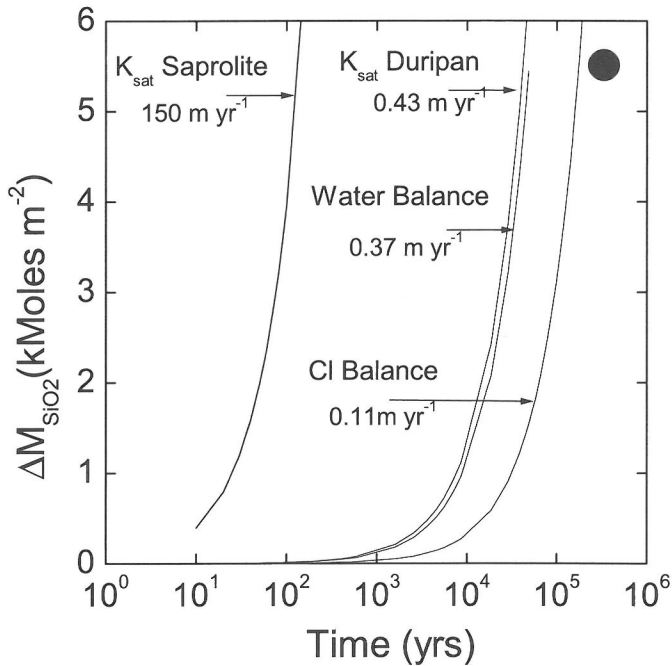


Fig. 11. Comparison of short- and long-term Si weathering rates for the Panola saprolite. The solid symbol corresponds to regolith mass loss  $\Delta M_{Si}$  calculated from changes in chemistry and profile age (Eqn. 4). Lines correspond to extrapolated weathering trajectories calculated from solute mass loss  $\Delta m_{Si}$  (Eqn. 5) and the indicated infiltration rates.

Slower unsaturated flow in the saprolite, estimated from watershed balances and from the saturated conductivity of the overlying less-permeable duripan produce trajectories that are more realistic, overestimating the Si loss from the saprolite by less than a factor of 10 (Fig. 11). Estimated Si fluxes based on Cl balances most clearly agree with long-term Si mobility (Fig. 11). An infiltration rate of  $4 \times 10^{-7} \text{ m s}^{-1}$  over  $3 \times 10^5$  years produces a calculated total Si loss of  $\Delta m_{Si} = 7.6 \times 10^3 \text{ moles m}^{-2}$ , which is comparable to the measured long-term loss of  $5.5 \times 10^3 \text{ moles m}^{-2}$ .

This study concludes that present day Si fluxes in pore waters are indistinguishable from long-term average Si fluxes derived from saprolite weathering over the last several hundred thousand years. This implies that parameters influencing Si weathering rates, such as precipitation, temperature, and vegetative cover, while not necessarily constant, have not varied enough to significantly impact Si leaching rates during this time. Similar close agreements between short- and long-term weathering fluxes have been reported for other saprolitic regoliths (Velbel, 1985; Pavich et al., 1995; White et al., 1998).

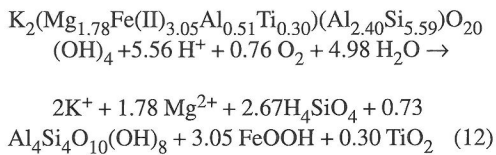
#### 4.5. Rates of Biotite Weathering

Dissolved Si in the pore waters of the Panola regolith is derived principally from silicate weathering reactions. The extent to which primary silicates are weathered can be calculated from mass balance considerations (White et al., 2001). The mass of weathered plagioclase is first calculated based on plagioclase stoichiometry, fresh bedrock Na concentrations (Table 2), and  $\tau_{Na}$  values for the regolith (Fig. 9B). Next, all of the Mg is similarly partitioned into the mica phases. It is not possible to distinguish computationally between muscovite and biotite because each mineral contains the same set of elements, i.e., K, Mg, Fe, Ti, Si, and Al, although at different concentrations. Based on petrographic and chemical evidence (Figs. 2 and 3), muscovite is assumed to be unreactive in the regolith and equal in concentration to that in the fresh bedrock. The change in Mg in the regolith is thereby apportioned solely to biotite (Velbel, 1985). The final step of the calculation is to distribute the remaining K into the K-feldspar phase.

Computations show that the amount of plagioclase lost in the saprolite is essentially constant with depth

and equal to the initial amount of plagioclase present in the unweathered Panola Granite (Fig. 12A, vertical line). Plagioclase is nearly completely converted to kaolinite at the weathering front in the underlying bedrock and is unavailable as a reactant in the overlying soil and saprolite (White et al., 2001). Approximately half of the K-feldspar weathers at the bedrock/saprolite interface (Fig. 12B), thus accounting for most of the K loss tabulated in Table 6. Losses of K-feldspar vary significantly in the overlying saprolite and soil. This may, in part, be an artifact attributable to compounding errors in the mass balance calculations, which first must distribute K into the muscovite and biotite phases before the mass of residual K-feldspar can be calculated. The overall trend in the data suggests that residual K-feldspar continues to weather, albeit at a slower rates in the overlying saprolite and soil.

Biotite losses can be calculated based on Mg distributions (Table 2 and Fig. 9B), which decrease consistently with decreasing depth in the regolith (Fig. 12C). Based on the biotite stoichiometry determined by microprobe analysis (Table 1), the epitaxial reaction of biotite to kaolinite can be written as follows



This reaction assumes that all of the Fe in the biotite is in the ferrous state, which is in accord with charge-balance constraints. For every mole of Mg lost, 0.56 moles of biotite have reacted. The diagonal line in

Fig. 12 C corresponds to a linear regression fit for depth versus biotite loss (slope  $b = 1.74 \times 10^{-2} \text{ m}^4 \text{ moles}^{-1}$  and  $r^2 = 0.90$ ). Under isovolumetric conditions, the mineral weathering rate is inversely proportional to the slope of the mineral distribution with depth; the shallower the slope, the more rapid the weathering reaction (White et al., 2001). The long-term dissolution rate constant for biotite,  $k_{\text{biotite}}$  ( $\text{moles m}^{-2} \text{ s}^{-1}$ ), can be derived from this relationship, such that

$$k^*_{\text{Biotite}} = \frac{w_{\text{reg}}}{b} \left( \frac{1}{\rho_{\text{reg}} f_{\text{biotite}} S_{\text{biotite}}} \right) \quad (13)$$

where  $w_{\text{reg}}$  ( $\text{m s}^{-1}$ ) is the rate of regolith formation, estimated to be  $7 \text{ m}/10^6 \text{ yrs}$  based on  $^{36}\text{Cl}$  age dating (Bierman et al., 1995). The terms in parentheses define the volumetric surface area of biotite ( $\text{m}^2 \text{ m}^{-3}$ ). The average saprolite density  $\rho_{\text{sap}} = 1.85 \times 10^6 \text{ g m}^{-3}$  (Table 2). The average volume fraction of biotite  $f_{\text{biotite}}$  present during regolith weathering is assumed to be 0.05, or one-half the fraction of biotite found in the fresh bedrock (Table 1). The specific surface area of the biotite is taken as the average of the BET analyses reported in Table 4 ( $5.0 \text{ m}^2 \text{ g}^{-1}$ ). The resulting long-term biotite dissolution rate constant is  $k_{\text{biotite}} = 2.8 \times 10^{-17} \text{ moles m}^{-2} \text{ s}^{-1}$ .

The dissolution rate constant for long-term biotite weathering in the Panola saprolite  $k_{\text{biotite}}$  is compared to both natural and experimental dissolution rates reported elsewhere in the literature (Table 8). Reported pH ranges, methods of surface area determination, and elemental basis for the biotite rate constants are also tabulated. The Panola rate is the slowest yet recorded for biotite weathering and is almost 5 orders

Table 8. Weathering rates of biotite measured in field and laboratory studies

log rate R moles $\text{m}^{-2} \text{ s}^{-1}$	pH	Location or experiment	Surface area	Basis of rate determination	
<i>Field</i>					
<b>-16.4</b>	<b>5.0 - 5.5</b>	<b>Panola, GA USA</b>	<b>BET</b>	<b>Mg regolith loss</b>	<b>This study</b>
-15.0	4.5	Luquillo Mtn., PR	BET	Mg solute flux	Murphy et. al., 1998
-14.0	4.5	Bear Brook, MA USA	Geometric	Si solute flux	Swoboda-Colberg & Drever (1993)
-13.0	6.0	Coweeta, NC USA	Geometric	Mg release	Velbel (1985)
<i>Laboratory</i>					
-11.9	4.5	experimental	BET	Cation release	Kalinowski & Schweda (1996)
-11.5	4.0 - 4.5	experimental	BET	K & Mg release	Sverdrup and Warfvinge (1995)
-11.4	4.5	experimental	Geometric	K release	Swoboda-Colberg & Drever (1993)
-10.7	5.0	experimental	BET	Mg release	Acker and Bricker (1992)

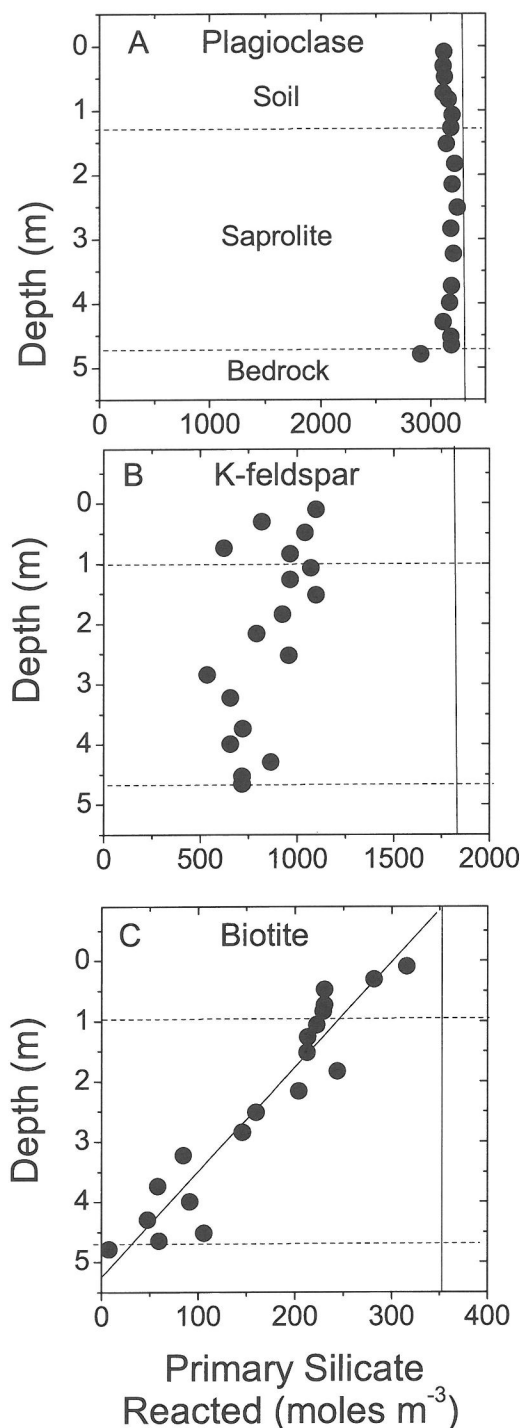


Fig. 12. Masses of primary silicates reacted in the Panola regolith. Vertical lines correspond to the initial protolith compositions. Diagonal line is the linear regression fit to the biotite weathering data

of magnitude slower than the fastest experimental rates, recorded by Acker and Bricker (1992).

In general, experimental rates of biotite weathering are faster than the natural weathering rates, as is commonly observed for most silicate minerals (White and Brantley, 1995; and papers therein). Much of the variation in reported rates are inevitably due to differences in methodologies used in the weathering studies. One of the most sensitive variables is specific surface area. Field studies by Velbel (1985) and Swodoba-Colberg and Drever (1993) used geometric surface areas, which in the case of naturally weathered silicates, have been shown to be 1 to 2 orders of magnitude less than BET surface areas (White and Peterson, 1990; Brantley et al., 1999). The only other natural biotite-weathering rate using BET surface areas was that for the Luquillo watershed in Puerto Rico (Murphy et al., 1998). This biotite rate, based on present day solute transport rates of Mg and K, is about 25 times faster than that at Panola. At least a part of this difference can be attributed to accelerated silicate weathering under significantly wetter and warmer climatic conditions in Puerto Rico (White et al., 1998).

#### 4.6. Solute Fluxes Related to Cation Exchange and Biotic Cycling

Biotite and K-feldspar weathering mobilizes Mg and K in the Panola regolith as indicated by long-term losses from the saprolite (Table 6). However, the solute concentrations of these elements decrease as functions of depth and residence times in the saprolite (Fig. 6), implying that significant sinks for these elements exist in the regolith. The roles of ion exchange and biological cycling are often neglected in attempts to explain such apparent discrepancies in weathering processes. The assumption most often made is that ion exchange is at equilibrium and no net gain or loss of cations occurs in the solute phase (White and Blum, 1995). Over long-term weathering, this assumption is clearly incorrect because the exchange capacity of the regolith increases as the percentage of clays and secondary oxides increase (Fig. 8). On a short-term basis, cation exchange disequilibrium can occur due to external perturbations, such as changes in climate, deforestation, and acid precipitation, all of which can potentially impact the pore water solutes in the Panola regolith.

At shallow soil depths, exchangeable Ca dominates over lesser amounts of Mg and K, and very low concentrations of Na (Fig. 8B). The regolith contains very little Ca due to the near-complete weathering of plagioclase at depth in the bedrock. High concentrations of exchangeable Ca in the shallow soils reflect the

preferential cycling and retention of Ca during biological cycling. Wet precipitation, which is relatively enriched in Ca (Table 3), is the ultimate source of much of this recycled Ca (Huntington et al., 2000). In the deeper soils and saprolite (>0.5 m), the proportions of Mg and K are much higher than Ca, a trend reflecting the diminished role of biological cycling and the increased role of chemical weathering. Exchangeable Mg is derived principally from biotite and K is derived from both biotite and K-feldspar (Fig. 12).

Total exchangeable Mg and K in the Panola regolith are 1.9 moles and 1.4 moles per m<sup>2</sup> of land surface, respectively (Fig. 8B). Based on the biotite weathering rate ( $k^*_{\text{biotite}} = 2.8 \times 10^{-17}$  moles m<sup>-2</sup> s<sup>-1</sup>), the time intervals required to replace this exchangeable Mg and K are 270 and 180 years, respectively. The actual replacement time for K is expected to be less due to an additional contribution from K-feldspar weathering. In contrast, pore water Mg and K concentrations produced by biotite weathering are limited to the fluid residence time in the regolith, which at a maximum is calculated to be 12 years (Eqn. 10). Resulting total solute Mg and K in pore waters, 0.083 and 0.093 moles per m<sup>2</sup> of land surface respectively, are correspondingly much less than the exchangeable Mg and K. The magnitude of these differences implies that solute concentrations are significantly impacted by even small perturbations in the cation exchange reservoir. Historically, the Panola watershed has been subjected both to past agricultural development (Huntington et al., 2000), and more recently, acidic precipitation (Shanley, 1992). Long-term cation exchange re-equilibration in response to these impacts could serve as a significant sink by which solute Mg and K, produced by silicate weathering, are effectively removed.

In many mass-balance studies in pristine watersheds, the forest ecosystem is assumed to be steady state, i.e., there is neither degradation nor aggradation. As discussed by Taylor and Velbel (1991) and Velbel (1995), the neglect of botanical factors in geochemical estimates of weathering stems from the misunderstanding of steady-state conditions in terms of temporal and spatial scales. On a watershed scale, biological cycling generally removes inorganic nutrients such as K, Mg, and Ca from the system, resulting in an underestimation of weathering rates by a factor 2 to 5 for these elements. Part of this net biologic loss can be attributed to net erosional loss of particulate organic matter that is not considered in solute mass-balance calculations. In addition, as discussed by Huntington (1995), the Panola watershed is considered an aggrading ecosystem in which the forest cover is recovering from logging and agricultural practices employed up to the earlier part of the twentieth century.

On the smaller regolith scale, the concept of closed- and open-system interaction between weathering and biologic uptake is also important (Burnham, 1989). In a closed system, biologic uptake of solutes resulting from mineral weathering is negligible. Forest fertility is maintained by low level atmospheric inputs and by efficient retention and recycling of these nutrients in near-surface soil horizons. This is the case for Ca cycling in the Panola soil (Huntington et al., 2000), and is demonstrated for Mg and K cycling in a parallel study of the tropical regolith in the Luquillo Mountains in Puerto Rico (White et al., 1998; Murphy et al., 1998). As at Panola, solute Mg and K levels are high in shallow Luquillo soil and low in the underlying shallow saprolite. However with increasing depth in the Luquillo saprolite, solute K and Mg increased linearly, denoting contributions from their stoichiometric release from biotite over progressively longer residence times. The deeper Luquillo regolith is closed to biological uptake of K and Mg produced by weathering due to the shallow rooting depth of the rainforest vegetation. This closed system cycling is consistent with other tropical environments in which soil mineral nutrient balances for vegetative covers are shown to be spatially consistent over differing bedrock types (Hamdan and Burnham, 1996).

In contrast to Luquillo, the Panola regolith is an example of an open system in which base cations, principally K and Mg released from biotite weathering in the saprolite, are removed due to biological uptake. In the Panola regolith, tree roots predominate in the soil horizon, but a lower density of roots is also observed to penetrate to the bedrock. The uptake by this deeper rooting system, coupled with the shallower thickness of saprolite, is sufficient to quantitatively remove mineral nutrients. Based on the biotite weathering

Table 9. Annual fluxes in the Panola Watershed (mmoles m<sup>-2</sup> yr<sup>-1</sup>)

	Si	K	Mg	Ca	Na
<b>Wet Precipitation</b>	0.0	0.1	0.18	0.08	6
<b>Weathering of biotite in saprolite</b>	4.8	2.5	2.3	0.0	0.0
<b>Vegetative Fluxes</b>					
Through fall <sup>1</sup>	na	36.5	7.2	12.9	6.6
Stem flow <sup>1</sup>	na	2.1	0.6	0.9	0.5
Foliar runoff <sup>1</sup>	na	149	83.3	112	2.6
<b>Stream Discharge</b>	67.6	1.8	8.2	12.1	32

<sup>1</sup>Cappellato et al. (1993) & Cappellato and Peters (1995).

rate ( $k^*_{\text{biotite}} = 3.9 \times 10^{-17}$  moles  $\text{m}^{-2} \text{s}^{-1}$ ), the annual solute flux of Mg and K from biotite weathering is 2.0 and 2.3  $\text{mmoles m}^{-2} \text{yr}^{-1}$ , respectively (Table 9). The annual export from the forest canopy to the soil surface in the forms of through fall, stem flow, and foliar deposition are also summarized in Table 9. The sum of the Mg and K fluxes are respectively 36 and 75 greater than are the corresponding fluxes from biotite weathering. At most, on an annual basis, biotite weathering can contribute 1 to 3% of the total K and Mg cycled through the biosphere. Soluble K and Mg, made available during chemical weathering of silicates, are immediately included in biologic uptake, which explains the lack of Mg and K in the saprolite pore waters.

## 5. CONCLUSIONS

The Panola regolith possesses unique features that optimize the comparison of past long-term weathering rates, based on solid-state compositions, with present short-term weathering rates based on solute fluxes. Unlike soils developed on bedrocks exposed to periods of relatively recent glaciation, the long duration of *in situ* isovolumetric weathering at Panola has produced a thick regolith, which has undergone significant mineral weathering and elemental mobility. These conditions are ideal for applying mass-balance constraints using conservative elements such as Zr, Ti, and Nb. The use of cosmogenic  $^{36}\text{Cl}$  to estimate the steady rate of regolith propagation permits the determination of long-term elemental and mineral weathering rates. As demonstrated, the weathering rate constant for biotite can be directly calculated from the rate of mineral loss with regolith depth. This rate is up to 5 orders of magnitude slower than rates for experimental biotite dissolution, implying significantly different reaction mechanisms and/or conditions.

Long-term weathering has led to the development of significant regolith structure that influences present day weathering, in particular, the duripan at the soil/saprolite boundary which strongly attenuates both fluid flow and mass transfer into the underlying saprolite. Such steady-state conditions permit characterizing solute fluxes based on pore water concentrations and regolith permeability determined from experimental conductivities and water and Cl mass balances. Fluid residence times on the order of a decade are contrasted to time spans of several hundred thousands of years for regolith weathering. However, when the respective Si losses in the regolith and pore waters are normalized with respect to these times, the Si weathering rates differ by less than a factor of two. This similarity in Si rates implies that past changes in the watershed, including climate, vegeta-

tion, and anthropogenic influences have not significantly influenced the rates of chemical weathering. The calculation of mineral dissolution rates based on increases in solute cation concentrations is not possible because, unlike the solid phases, these species decrease with depth and residence times in the regolith. When the magnitude of the weathering rates are compared to cation exchange capacities and biologic cycling, it is apparent that small variations in these parameters can effectively eliminate the solute cation weathering signature.

*Acknowledgements*—The Water Energy Biogeochemical Budgets (WEBB) program of the Water Resources Division of the U. S. Geological Survey funded this work. The authors express their gratitude to Drs. Michael Velbel, James Drever, Susan Anderson, and Roland Hellmann for helpful reviews and suggestions pertaining to this paper.

*Editorial handling*: Roland Hellmann

## REFERENCES

- Acker J. G. and Bricker O. P. (1992) The influence of pH on biotite dissolution and alteration kinetics at low temperature. *Geochim. Cosmochim. Acta* **56**, 3073-3092.
- Al-Kanani T. and MacKenzie A. F. (1990) Phosphate hydrolysis in mineral fractions of soils, goethite, kaolinite and montmorillonite. *Soil Science* **149**, 239-247.
- April R., Newton R., and Coles L. T. (1986) Chemical weathering in two Adirondack watersheds: Past and present-day rates. *Geol. Soc. Amer. Bull.* **97**, 1232-1238.
- Bierman P., Gillespie A., Caffee M., and Elmore D. (1995) Estimating erosion rates and exposure ages with  $^{36}\text{Cl}$  produced by neutron activation. *Geochim. Cosmochim. Acta* **59**, 3779-3798.
- Brantley S. L., White A. F., and Hodson M. E. (1999) Surface area of primary silicate minerals. In *Growth, Dissolution and Pattern Formation in Geosystems* (eds. B. Jamtveit and P. Meakin). Kluwer Academic Publishers, Dordrecht. pp 291-326.
- Brimhall G. H. and Dietrich W. E. (1987) Constitutive mass balance relations between chemical composition, volume, density, porosity, and strain in metasomatic hydrochemical systems: Results on weathering and pedogenesis. *Geochim. Cosmochim. Acta* **51**, 567-587.
- Buffle J. (1988) *Complexation Reactions in Aquatic Systems: An Analytical Approach*. John Wiley and Sons, New York.
- Buol S. W. and Weed S. B. (1991) Saprolite-soil transformations in the Piedmont and Mountains of North Carolina. *Geoderma* **51**, 15-28.
- Burnham C. P. (1989) Pedological processes and nutrient supply from parent material in tropical soils. In *Mineral Nutrients in Tropical Forest and Savanna Ecosystems* (ed. J. Proctor). Blackwell Scientific Publications, Oxford. pp. 27-40.
- Burns D. A. (1998) The hydrochemical evolution of stormflow in a forested Piedmont catchment, Ph.D. thesis, State University of New York.
- Burns D. A., Hooper R. P., McDonnell J. J., Freer J. E., Kendall C., and Beven K. (1998) Base cation concentra-

- tions in subsurface flow from a forested hillslope-The role of flushing frequency. *Water Resources Res.* **34**, 3535-3544.
- Cappellato R., Peters N. E., and Ragsdale H. L. (1993) Acidic atmospheric deposition and canopy interactions of adjacent deciduous and coniferous forests in the Georgia Piedmont. *Canadian J. Forest Res.* **23**, 1114-1124.
- Cappellato R. and Peters N. P. (1995) Dry deposition and canopy leaching in deciduous and coniferous forests of the Georgia Piedmont: an assessment of a regression model. *J. Hydrology* **169**, 131-150.
- Chadwick O. A., Brimhall G. H., and Hendricks D. M. (1990) From black box to a grey box: A mass balance interpretation of pedogenesis. *Geomorphology* **3**, 369-390.
- Cleaves E. T. (1993) Climatic impact on isovolumetric weathering of a coarse-grained schist in the northern Piedmont Province of the central Atlantic states. *Geomorphology* **8**, 191-198.
- Dixon J. B. and Weed S. B. (1977) *Minerals in Soil Environments*. Soil Science Society of America, Madison.
- Dong H., Peacor D. R., and Murphy S. F. (1998) TEM study of progressive alteration of igneous biotite to kaolinite throughout a weathered soil profile. *Geochim. Cosmochim. Acta* **62**, 1881-1887.
- Driscoll C. T., van Breemen N., and Mulder J. (1985) Aluminum chemistry in a forested spodosol. *Soil Sci. Soc. Am. J.* **49**, 437-444.
- Eriksson E. and Kunakasen V. (1969) Chloride concentrations in groundwater, recharge rate and rate of deposition of chloride in the Israel Coastal Plain. *J. Hydrology* **7**, 178-197.
- Flury M. and Fluhler H. (1994) Susceptibility of soils to preferential flow of water: A field study. *Water Resources Res.* **30**, 1945-1954.
- Grant W. H. (1975) Chemical Weathering of Panola Adamellite with special reference to apatite. *Southeastern Geology* **17**, 15-25.
- Hamdan J. and Burnham C. P. (1996) The contribution of nutrients from parent material in three deeply weathered soils of Peninsular Malaysia. *Geoderma* **74**, 219-233.
- Higgins M. W., Atkins R. L., Crawford T. J., Crawford R. F., III, Brooks R., and Cook R. (1988) The structure, stratigraphy, tectonostratigraphy and evolution of the southernmost part of the Appalachian orogen. *U. S. Geological Survey Prof. Paper* **1475**, 173p.
- Hillel D. (1982) *Introduction to Soil Physics*. Academic Press, San Francisco.
- Huntington T. G. (1995) Carbon sequestration in an aggrading forest ecosystem in the Southeastern USA. *Soil Sci. Soc. Am. J.* **59**, 1459-1467.
- Huntington T. G., Johnson A. H., and Schwartzman T. N. (1990) Mechanical vacuum extraction vs. batch equilibrium for estimation of exchangeable cations. *Soil Sci. Soc. Am. J.* **54**, 381-385.
- Huntington T. G., Hooper R. P., Peters N. E., Bullen T. D., and Kendall C. (1993) Water, energy and biogeochemical budgets investigation at Panola Mountain Research Watershed, Stockbridge, Georgia - A research plan. *U. S. Geological Survey Open File Report* **93-55**, 49.
- Huntington T. G., Blum A. E., and White A. F. (1994) Migration of a bromide tracer in a forest soil in the Georgia Piedmont. *EOS* **75**(16), 150.
- Huntington T. G., Hooper R. P., Johnson C. E., Aulenbach B. T., Cappellato R., and Blum A. E. (2000) Calcium depletion in forest ecosystems of the southeastern United States. *Soil Sci. Soc. Amer. J.* **64** 1845-1858.
- Jardine P. M., Parker J. C., and Zelazny L. W. (1985) Kinetics and mechanisms of aluminum adsorption on kaolinite using two-site non-equilibrium transport model. *Soil. Sci. Soc. Am. J.* **49**, 867-872.
- Jeong G. Y. (1998) Vermicular kaolinite epitactic on primary phyllosilicates in the weathering profiles of anorthosite. *Clays & Clay Minerals* **46**, 509-520.
- Kalinowski B. E. and Schweda P. (1996) Kinetics of muscovite, phlogopite and biotite dissolution and alteration at pH 1-4, room temperature. *Geochim. Cosmochim. Acta* **60**, 367-385.
- Kenoyer G. J. and Bowser C. J. (1992) Groundwater chemical evolution in a sandy silicate aquifer in northern Wisconsin 2. Reaction modeling. *Water Resources Res.* **28**, 591-600.
- Kirkwood S. E. and Nesbitt H. W. (1991) Formation and evolution of soils from an acidified watershed: Plastic Lake, Ontario, Canada. *Geochim. Cosmochim. Acta* **55**, 1295-1308.
- Klute A. and Dirksen C. (1986) Hydraulic conductivity and diffusivity: Laboratory methods. In *Methods of Soil Analysis* (ed. A. Klute). Soil Sci. Soc. America, Madison. pp. 687-699.
- Kretzschmar R., Robarge W. P., Amoozegar A., and Vepraskas M. J. (1997) Biotite alteration to halloysite and kaolinite in soil-saprolite profiles developed from mica schist and granite gneiss. *Geoderma* **75**, 155-170.
- Land M., Ingri J., and Ohlander B. (1999) Past and present weathering rates in northern Sweden. *Applied Geochem.* **14**, 761-774.
- Lee M. R. and Parsons, P. I. (1999) Biomechanical and biochemical weathering of lichen-encrusted granite: Textural controls on organic-mineral interactions and deposition of silica-rich layers. *Chem. Geology* **161**, 385-397.
- Levy G. J., van der Watt H. H., Shainberg I., and Plessis H. M. (1988) Potassium-calcium exchange and sodium-calcium exchange on kaolinite and kaolinitic soils. *Soil Sci. Soc. Am. J.* **52**, 1259-1264.
- Markewich H. W. and Pavich M. J. (1991) Soil chronosequence studies in temperate to subtropical, low-latitude, low-relief terrain with data from the eastern United States. *Geoderma* **51**, 213-239.
- Mehra O. P. and Jackson M. L. (1960) Iron oxide removal from soils and clays by a dithionite-citrate system buffered with sodium bicarbonate. In *Proceedings 7th National Conference on Clays and Clay Minerals* (ed. A. Swineford). Pergamon Press, New York. pp. 317-327.
- Murphy S. F., Brantley S. L., Blum A. E., White A. F., and Dong H. (1998) Chemical weathering in a tropical watershed, Luquillo Mountains, Puerto Rico. II Rate and mechanism of biotite weathering. *Geochim. Cosmochim. Acta* **62**, 227-243.
- Nixon R. A., III. (1981) Rates and mechanisms of chemical weathering in an organic environment at Panola Mountain, Georgia. Ph.D. thesis, Emory University, GA (USA).
- O'Brien E. L. and Buol S. W. (1984) Physical transformations in a vertical soil-saprolite sequence. *Soil Sci. Amer. J.* **48**, 354-357.
- Pačes T. (1986) Rates of weathering and erosion derived from mass balance in small drainage basins. In *Rates of Chemical Weathering of Rocks and Minerals* (eds. S. M. Colman & D. P. Dethier). Academic Press, San Francisco. pp. 531-550.
- Pavich M. J., Brown L., and Valette-Silver H. N. (1995) <sup>10</sup>Be analysis of a Quaternary weathering profile in the Virginia Piedmont. *Geology* **13**, 39-41.

- Schoenberger P. J., Amoozegar A., and Buol S. W. (1995) Physical properties of a soil and saprolite continuum at three geomorphic positions. *Soil Sci. Soc. Amer. J.* **59**, 1389-1397.
- Schroeder P. A. and Melear N. D. (1999) Stable carbon isotope signatures preserved in authigenic gibbsite from a forested granitic regolith: Panola Mt. Georgia, USA. *Geoderma* **91**, 261-279.
- Schulz M. S. and White A. F. (1999) Chemical weathering in a tropical watershed, Luquillo Mountains, Puerto Rico III: Quartz dissolution rates. *Geochim. Cosmochim. Acta* **63**, 337-350.
- Shanley J. B. (1992) Sulfate retention and release in soils at Panola Mountain, Georgia. *Soil Science* **153**, 499-508.
- Simpson G. G. (1986) Hydraulic characteristics of soil-saprolite profiles from North Carolina Piedmont. *Proc. 29th Meeting of the Soil Sci. Soc., North Carolina*, 147-200.
- St. Pierre T. G., Singh B., Webb J., and Gilkes B. (1992) Mössbauer spectra of kaolins from south-western Australia. *Clay and Clay Minerals* **40**, 341-346.
- Stonestrom D. A., White A. F., and Akstin K. C. (1998) Determining rates of chemical weathering in soils-solute transport versus profile evolution. *J. Hydrology* **209**, 331-345.
- Sverdrup K. and Warfvinge P. (1995) Estimating field weathering rates using laboratory kinetics. In *Chemical Weathering Rates of Silicate Minerals* (eds. A. F. White and S. L. Brantley). Reviews in Mineralogy **31**, Mineralogical Society of America, Washington, D.C. pp. 485-541.
- Swodoba-Colberg N. G. and Drever J. D. (1993) Mineral dissolution rates in plot-scale field and laboratory experiments. *Chem. Geology* **105**, 51-69.
- Taylor A. B. and Velbel M. A. (1991) Geochemical mass balances and weathering rates in forested watersheds of the southern Blue Ridge II. Effects of botanical uptake terms. *Geoderma* **51**, 29-50.
- Vapraskas M. J. and Williams J. P. (1995) Hydraulic conductivity of saprolite as a function of sample dimensions and measurement technique. *J. Soil Sci. Amer. J.* **59**, 975-981.
- Velbel M. A. (1985) Geochemical mass balances and weathering rates in forested watersheds of the southern Blue Ridge. *Amer. J. Sci.* **285**, 904-930.
- Velbel M. A. (1995) Interaction of ecosystem processes and weathering processes. In *Solute Modelling in Catchment Systems* (ed. S. T. Trudgill). John Wiley and Sons, New York. pp. 193-209.
- White A. F. (1995) Chemical weathering rates in soils. In *Chemical Weathering Rates of Silicate Minerals* (eds. A.F. White and S.L. Brantley). Reviews in Mineralogy **31**, Mineralogical Society of America, Washington, D.C. pp. 407-458.
- White A. F. and Blum A. E. (1995) Effects of climate on chemical weathering rates in watersheds. *Geochim. Cosmochim. Acta* **59**, 1729-1747.
- White A. F. and Brantley S. L. (1995) Chemical weathering rates of silicate minerals: An overview. In *Chemical Weathering Rates of Silicate Minerals* (eds. A.F. White and S.L. Brantley). Reviews in Mineralogy **31**, Mineralogical Society of America, Washington, D.C. pp. 1-22.
- White A. F. and Claassen H. C. (1978) Dissolution kinetics of silicate rocks, application to solute modeling. In *Speciation, Sorption, Solubility and Kinetics in Aqueous Systems* (ed. E. Jenne). American Chemical Society Symposium Series **93**, American Chemical Society, Washington, D.C. pp. 771-793.
- White A. F. and Peterson M. L. (1990) Role of reactive surface area characterization in geochemical models. In *Chemical modeling of aqueous systems II* (eds. D. C. Melchior and R. L. Bassett), American Chemical Society Symposium Series **416**, American Chemical Society, Washington, D.C. pp. 771-793.
- White A. F., Blum A. E., Schulz M. S., Bullen T. D., Harden J. W., and Peterson M. L. (1996) Chemical weathering of a soil chronosequence on granitic alluvium 1. Reaction rates based on changes in soil mineralogy. *Geochim. Cosmochim. Acta* **60**, 2533-2550.
- White A. F., Blum A. E., Schulz M. S., Vivit D. V., Larsen M., and Murphy S. F. (1998) Chemical weathering in a tropical watershed, Luquillo Mountains, Puerto Rico: I. Long-term versus short-term chemical fluxes. *Geochim. Cosmochim. Acta* **62**, 209-226.
- White A. F., Blum A. E., Bullen T. D., Vivit D. V., Schulz M., and Fitzpatrick J. (1999a) The effect of temperature on experimental and natural weathering rates of granitoid rocks. *Geochim. Cosmochim. Acta* **63**, 3277-3291.
- White A. F., Bullen T. D., Vivit D. V., and Schulz M. S. (1999b) The role of disseminated calcite in the chemical weathering of granitoid rocks. *Geochim. Cosmochim. Acta*, **63**, 1939-1953.
- White A. F., Bullen, T. D., Schulz M. S., Blum A. E., Huntington T. G., and Peters N. E. (2001) Differential rates of feldspar weathering in granitic regoliths. *Geochim. Cosmochim. Acta* **65**, 847-869.

